

Review

# Novel Nitride Materials Synthesized at High Pressure

Pei Wang<sup>1,2,\*</sup>, Shanmin Wang<sup>2</sup>, Yongtao Zou<sup>3</sup>, Jinlong Zhu<sup>2</sup>, Duanwei He<sup>4</sup>, Liping Wang<sup>1,\*</sup> and Yusheng Zhao<sup>1,2,\*</sup>

- <sup>1</sup> Academy for Advanced Interdisciplinary Studies & Shenzhen Engineering Research Center for Frontier Materials Synthesis at High Pressures, Southern University of Science and Technology (SUSTech), Shenzhen 518055, China
  - <sup>2</sup> Department of Physics & Shenzhen Engineering Research Center for Frontier Materials Synthesis at High Pressures, Southern University of Science and Technology (SUSTech), Shenzhen 518055, China; wangsm@sustech.edu.cn (S.W.); zhujl@sustech.edu.cn (J.Z.)
  - <sup>3</sup> College of Engineering Physics, and Center for Advanced Material Diagnostic Technology, Shenzhen Technology University, Shenzhen 518118, China; zouyongtao@sztu.edu.cn
  - <sup>4</sup> Institute of Atomic and Molecular Physics, Sichuan University, Chengdu 610065, China; duanweihe@scu.edu.cn
- \* Correspondence: wangp@sustech.edu.cn (P.W.); wanglp3@sustech.edu.cn (L.W.); zhaoy@sustech.edu.cn (Y.Z.)

**Abstract:** Nitride materials including conventional manmade superhard light-element nitrides, such as cubic boron nitride (cBN), cubic silicon nitride ( $\gamma$ -Si<sub>3</sub>N<sub>4</sub>), and carbonitrides, have been extensively used for machining (e.g., turning, cutting, grinding, boring, drilling) and coating of ferrous alloys due to their remarkable performances of high rigidity, high melting-point, and prominent chemical and thermal stabilities. However, to some degree, superhard nitrides merely compensate for the adverse limitations of diamond: reaction (with iron), oxidation, and graphitization at moderate temperatures; they are still unable to dominate the market owing to their relatively low hardness when compared to diamond. Therefore, recent efforts toward the preparation of nitride materials with outstanding mechanical performance and chemical inertness have focused on synthesizing ternary light-element nitride compounds and harvesting the effect of work hardening through microstructure manipulations. These new light-element nitrides are potential candidates to displace diamond in the cutting business. On the other hand, incorporation of transition-metal atoms into the dinitrogen triple-bond can form novel hard transition-metal nitride alloys (TMNAs), such as Mo-N, W-N, Pt-N, Ir-N, Os-N, etc., which are potential candidates for the cutting, coating, and polishing of iron-group metals. However, synthesis of high-crystallinity and stoichiometric TMNAs via traditional routes is challenging, since the embedded nitrogen in the transition-metal lattice is thermodynamically unfavorable at ambient condition. A novel approach involving ion-exchange reactions under moderate pressure and temperature has been developed in recent years for preparation of well-crystallized stoichiometric TMNAs, which have quickly been realized as emergent materials in electronics, catalysts, and superconductors as well.

**Keywords:** nitrides; high pressure; superhard; transition-metal nitrides



**Citation:** Wang, P.; Wang, S.; Zou, Y.; Zhu, J.; He, D.; Wang, L.; Zhao, Y. Novel Nitride Materials Synthesized at High Pressure. *Crystals* **2021**, *11*, 614. <https://doi.org/10.3390/cryst11060614>

Academic Editor: Cyril Cayron

Received: 13 April 2021

Accepted: 25 May 2021

Published: 29 May 2021

**Publisher's Note:** MDPI stays neutral with regard to jurisdictional claims in published maps and institutional affiliations.



**Copyright:** © 2021 by the authors. Licensee MDPI, Basel, Switzerland. This article is an open access article distributed under the terms and conditions of the Creative Commons Attribution (CC BY) license (<https://creativecommons.org/licenses/by/4.0/>).

## 1. Introduction

Diamond, as the hardest material known to mankind—its hardness is more than twice as high as that of the second hardest material, cubic boron nitride (cBN)—has widespread applications in industry [1–11]. As a wonder material with outstanding mechanical properties, diamond is ostensibly expected to serve as a universal cutting tool. However, chemical reactions with iron-group metals at moderate temperatures directly give rise to its failure in processing ferrous materials [12]. It is well known that light-element nitride materials (e.g., cBN) having a crystal structure analogous to that of diamond are potential candidates with outstanding mechanical properties and

thermal stability to turn ferrous alloys [12–15]. Searching for novel nitride materials with mechanical performance rivaling diamond and excellent chemical and thermal stability has therefore been a motivating and active area of research.

Nitride materials with diamond-like structure have been extensively studied using theoretical calculation methods [16–18]. However, unlike diamond, superhard nitride materials predicted by means of first-principles calculation, which like diamond are metastable at ambient conditions, have rarely been found in nature. Thanks to the development of ultra-high-pressure ( $P$ ) techniques, such as the large-volume multi-anvil apparatus [19–24] and the laser-heated diamond anvil cell (LH-DAC) [25], in the past few decades, most light-element nitride materials predicted by theoretical modeling have been synthesized experimentally using high-pressure devices. For instance, cBN was prepared from the phase transformation of hexagonal boron nitride (hBN) under extreme conditions of high pressure and high temperature ( $T$ ) [5]. Much later, nitrides predicted to be even harder than diamond, such as  $B_{13}N_2$ ,  $BC_2N$ ,  $BC_4N$ ,  $\gamma$ - $Si_3N_4$ , and carbonitrides [9,11,13,14,19,26–29], were also synthesized. These binary and ternary nitride compounds are characterized by short and strong  $sp^3$  covalent bonds between light elements (boron, carbon, oxygen, and silicon, etc.) and nitrogen, similar to carbon–carbon bonding in diamond (see Figure 1). Covalently bonded atoms in these nitrides form three-dimensional (3-D) networks of high symmetry with a high atomic density like in diamond and extreme resistance to external compression and shear, leading to some excellent mechanical properties [2,6]. Hence, although synthetic nitride materials having higher hardness than that of diamond have not yet been found, these materials are still competitive in many practical industrial applications, such as drilling, coating, and cutting. For example, cBN has only half the hardness of diamond, yet it is indeed the best-known material for polishing and cutting ferrous alloys and cemented carbide composites, where the chemical reaction and graphitization render diamond unstable and ineffective. The diamond–cBN alloy recently synthesized via mechanical alloying at high pressure and temperature is a universal cutting material, because it can be applied to high-speed cutting of both granite and steel [12], which proves that diamond has the potential of being applied to machining ferrous metals via nitride alloying upon surface treatment. Additionally, based on the Hall–Petch effect, much improved mechanical strength is achieved through the grain-size reduction or work hardening [30,31]. For example, nano-twinned cBN and submicron-cBN (sm-cBN) can be as hard as diamond, and remarkably, have a fracture toughness several-fold higher than that of diamond [3,7,32]. Twin and grain boundaries hinder the movements of dislocations during compressional and shear deformation, resulting in the high hardness and toughness of twinned materials and those with reduced grain-size.

On the other hand, it is realized that coupling small and covalent-bonding nitrogen atoms with closely packed transition metals that have high densities of valence electrons (molybdenum, platinum, iridium, osmium, etc.) could result in dramatic changes in physical properties of metals and lead to enhanced resistance to elastic and plastic deformations [2,6] and hence improved mechanical strength for resultant hard/superhard transition-metal nitride alloys (TMNAs). For instance,  $\delta$ -MoN has a bulk modulus of 372 GPa and a Vickers hardness of 30 GPa [33], both values much larger than those of its parent metal molybdenum (267 GPa and 2.2–3.6 GPa, respectively) [34,35]. However, it is extremely difficult to synthesize stoichiometric TMNAs of high-crystallinity with a nitrogen-to-metal ratio far greater than unity through traditional preparation methods [36–39]. At ambient pressure, TMNAs are generally synthesized by heating metals or their compounds in an ammonia ( $NH_3$ ) atmosphere or via vapor deposition and epitaxial growth methods. These methods suffer from long duration, poor production, low crystallinity, non-stoichiometry, and incompleteness of reaction. Recently, the preparation of nitride alloys has made substantial progress due to a new approach involving ion-exchange reactions under high pressure, temperature conditions suitable for industrial production [40,41]. Here, the ion-exchange reaction is launched by supplying new ions to a template compound. In this type of chemical reactions, the ions in the parent compound

spread out from the lattice and become solvated by solvents, while the substituted ions are incorporated into the lattice via internal diffusion [40,41]. High-crystallinity bulk nitride alloys, such as GaN, MoN,  $W_2N_3$ , CrN, VN,  $MoN_2$ , etc., have been synthesized using a large-volume cubic press, and their intrinsic mechanical properties (e.g., hardness, compressibility, and toughness) have been further characterized using ion-exchange reaction methods [40–44].

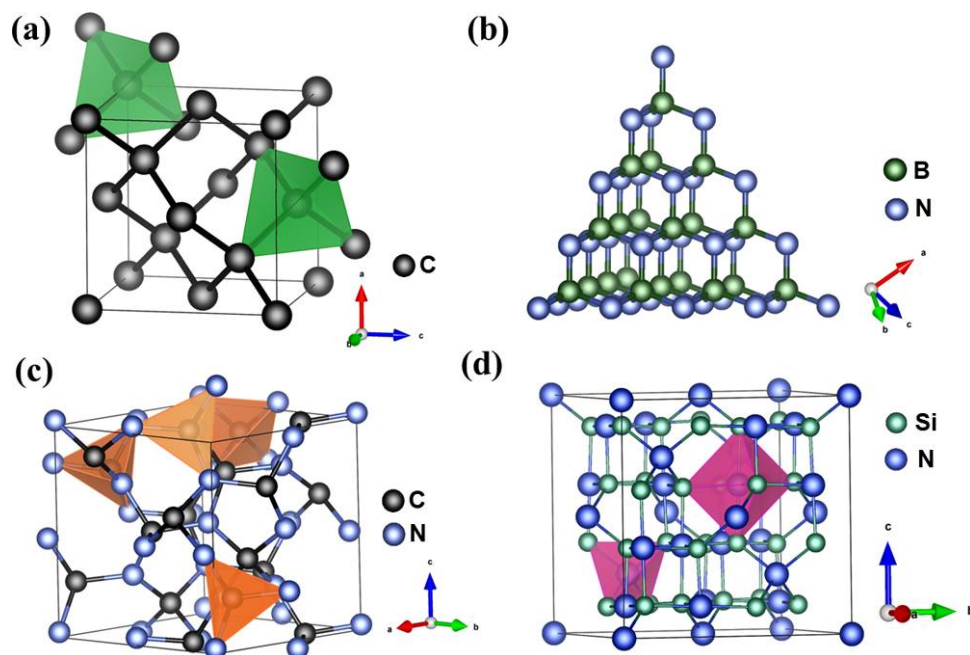


**Figure 1.** Crystal structures of (a) diamond, (b) cBN, (c) cubic  $C_3N_4$  (I-43d, ICSD 83263), and (d)  $\gamma$ - $Si_3N_4$  (cubic phase,  $Fd\bar{3}m$ , ICSD 97566), all of which are characterized by short and strong  $sp^3$  covalent bonds constituting a three-dimensional network of high-symmetry with a high atomic density. For these materials, carbon atoms are shown in black, boron atoms in green-gray, nitrogen atoms in blue, and silicon atoms in green.

In this paper, we mainly focus on reviewing recent advances in the preparation of nitride materials for machining technology and discussing challenges and opportunities in this important subfield for emergent materials. This article will draw forth some perspectives on the following several aspects: continuous improvement of large volume high-pressure synthesis technologies, understanding of the intrinsic and extrinsic nature of hard and superhard materials, designing and preparing potential superhard phases or composites, and harvesting the effect of work hardening through microstructure manipulations.

## 2. Preparation Technology of Nitride Materials Using Large-Volume Press at Static High Pressure

High-pressure processing is emerging as an effective and leading tool for synthesizing novel nitride materials possessing desirable mechanical and chemical properties and for improving the materials performances through microstructure and grain-size manipulations [3,4,7,8,32,45]. Large-Volume Press (LVP), as an indispensable technique, plays a crucial role in high-pressure research. LVPs were developed and put into use in the 1950s [46–48]; they are largely devoted to producing high pressures on bulk specimens that undergo designed synthesis reactions and notably to making diamond and cBN [1,5]. Today, a majority of synthetic diamond powder produced each year in the world is made by use of a hinge-type cubic press (DS  $6 \times 6 - 60$  MN) made in China (see Figure 2). Some novel nitride alloys such as CrN, VN,  $W_2N_3$ , and MoN with high-crystallinity have been synthesized using the same type of apparatus at moderate pressures and temperatures [40–44]. In order to attain higher pressures, double-stage multi-anvil apparatus of

various types have been developed, such as DIA-type (Osugi et al., 1964) [48], Kawai-type (Kawai and Endo, 1970) [24], and Walker-type [20] (one of split-cylinder type; Walker et al., 1990) multi-anvil apparatus.

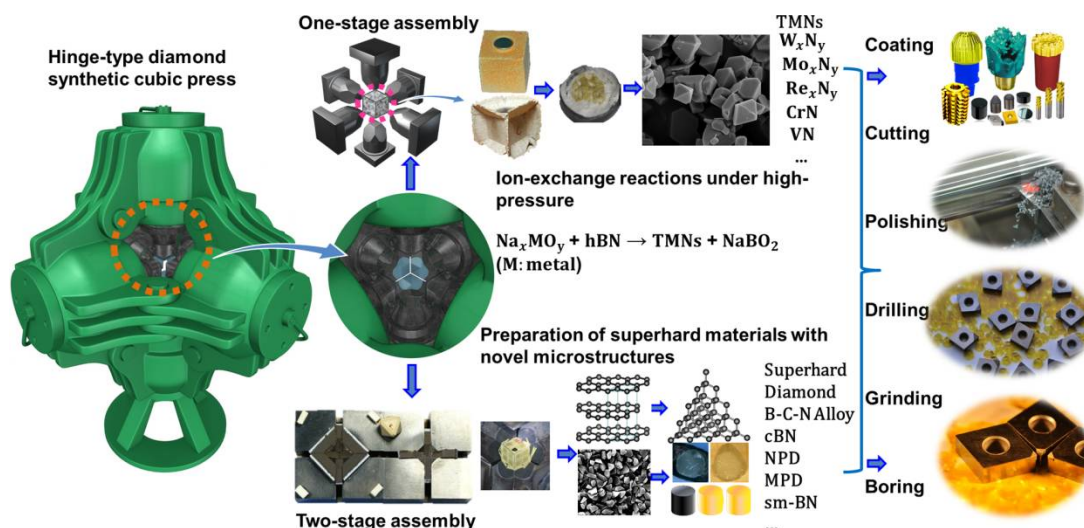


**Figure 2.** Schematic illustrations of the preparation of novel transition metal nitride alloys and superhard light-element nitride materials with two different sets of experimental assemblies involving one-stage assembly with pressure transmitting medium of pyrophyllite and two-stage assembly with pressure transmitting medium of MgO on basis of a hinge-type cubic press.

The above-mentioned double-stage multi-anvil apparatus are widely used for in-situ high-pressure research in conjunction with synchrotron radiations on material synthesis and characterization, but their applications for large-scale industrial production are somewhat limited due to high operational costs. Therefore, to synthesize with fast turnaround the bulk hard and superhard materials at low costs, we have developed three new types of sample assemblies based on two-stage hinge-type cubic press. As shown in Figure 2, the sample assembly (14/8, 12/6, or 10/4) [49,50], which is constitutive of a magnesium oxide (MgO) octahedron (edge-length of 14, 12, or 10 mm, respectively), a zirconia (ZrO<sub>2</sub>) sleeve as thermal insulator, and a cylindrical metal heater (Ta, Mo, Re, or Pt), is compressed by eight 18 mm cubic WC anvils with truncated corners (truncation edge-length of 8, 6, and 4 mm for each sample assembly, respectively). Pressures are estimated on the basis of phase changes in ZnS, ZnTe, and GaAs at room temperature [51]. A Pt6%Rh–Pt30%Rh or W5%Re–W25%Re thermocouple with a precision of about ±10 °C is used to measure the temperatures in situ. The obtained upper pressure limits for 14/8, 12/6, and 10/4 assemblies reach up to 16, 19, and 22 GPa, respectively, and the peak temperature approaches 2500 °C [12,21,49,50,52,53]. The recovered cylindrical samples have both diameter and height of about 3 mm. Employing two-stage multi-anvil apparatus has dramatically extended the LVP pressure range and laid the foundation for making the next-generation hard and superhard nitride alloying materials under extreme conditions. Numerous superhard materials, such as nano polycrystalline diamond (NPD) [53], micron-grained polycrystalline diamond (MPD) [54], sub-micron cBN (sm-cBN) [32], superhard composites of γ-Si<sub>3</sub>N<sub>4</sub> and diamond [55], and superhard B–C–N materials or solid solutions [12,56], have been successfully prepared using the double-stage high-pressure technique ground on the hinge-type cubic press.

### 3. Preparation of Light-Element Nitrides: Challenges and Opportunities

Diamond and cBN as the first-generation superhard materials have acquired massive industrial applications, but both have intrinsic shortcomings [12–14,57]. Diamond is not sufficiently competent in high-speed turning of ferrous materials owing to its mean chemical inertness, while cBN has only around half the hardness of diamond [6–8,12–14,57].

Hence, the next-generation superhard materials are desired to possess both high hardness and excellent thermal stability. In the past few decades, extensive experimental and theoretical trials have been applied to searching for B–C–N ternary compounds or their solid solutions [9,12–16,56–61], which are anticipated to be thermally and chemically more firm than diamond and more rigid than cBN, and would therefore be better materials for machining ferrous alloys. To acquire superhard materials with performances rival or even beyond those of diamond and cBN, researchers have made great endeavors to synthesize strongly covalent and high atomic-density compounds in light-elements B–C–N–O–Si–P system for scientific and industrial applications, with some significant achievements such as triumphant synthesis of nano polycrystalline diamond (NPD) [4,53], nano polycrystalline cubic boron nitride (NPcBN) [7,8,45], and B–C–N ternary compounds or alloys [12–16,56–61].

It is well known that molecular nitrogen is chemically very stable due to the strong covalent triple bonds between two nitrogen atoms; hence, synthesis of nitride materials is challenging via conventional methods. Simultaneous high-pressure and high-temperature has been proven to be a valid method for synthesizing novel nitride materials with excellent chemical stability and mechanical performance, such as cBN and  $\gamma$ -Si<sub>3</sub>N<sub>4</sub>. Solozhenko et al. first reported the synthesis of a cubic BC<sub>2</sub>N phase in both a laser-heated diamond-anvil cell (DAC) and multi-anvil press at about 26 GPa/2200 °C [13,57], using graphite-like BC<sub>2</sub>N and BC<sub>4</sub>N as the starting materials. The single phase BC<sub>2</sub>N has a hardness value of 76 GPa, which is comparable to that of diamond. Subsequently, Zhao et al. reported the preparation of good-sintered millimeter-sized chunks of superhard BC<sub>2</sub>N and BC<sub>4</sub>N at 20 GPa/1900 °C using nearly amorphous ball-milled mixtures of graphite and hBN [14]. The hardness for the BC<sub>2</sub>N and BC<sub>4</sub>N compacts at a load of 9.8 N was about 62 and 68 GPa (Figure 3), respectively, which rival single-crystal diamond (85 GPa) and are much higher than that of cBN (47 GPa) at the same loading force. The nano-structured B–C–N materials with superb performance are therefore ultrahard material whose Vickers hardness surpasses 40 GPa.

However, novel cubic C<sub>3</sub>N<sub>4</sub> predicted by first principles calculations to be harder than diamond has not been successfully synthesized so far [9,11,16–18]. There are also insufficient experimental data on B<sub>6</sub>N to constrain its mechanical properties and chemical stability [62]. Among the synthetic nitride materials,  $\gamma$ -Si<sub>3</sub>N<sub>4</sub> (H<sub>V</sub>: 30 GPa) [28,29], BeP<sub>2</sub>N<sub>4</sub> [63], Si<sub>3</sub>B<sub>3</sub>N<sub>7</sub> [64],  $\beta$ -BP<sub>3</sub>N<sub>6</sub> [65], and cubic P<sub>3</sub>N<sub>5</sub> (H<sub>V</sub>: 9.7 GPa) [66,67] all have hardness much lower than that of cBN (H<sub>V</sub> for single crystal: 47 GPa) [13,14,68]. More efforts are needed to improve the high-pressure synthesis technology and discover single-phase nitride materials that are harder than diamond.

Mechanic performance and chemical stability of bulk nitride materials can be improved through grain-size reduction and microstructure manipulation, which have been commonly employed to strengthen metal alloys; for instance, repeatedly strained aluminum can obtain higher values of hardness and fracture toughness [69,70]. Dubrovinskaia et al. synthesized superhard aggregated boron nitride nanocomposites (ABNNCs) with the maximum hardness of 85(3) GPa using a multi-anvil press [8]. It is proposed that the Hall–Petch and the quantum confinement effects play a critical role in increasing the hardness of aggregated boron nitride nanocomposites [3,7,30,31]. Moreover, ABNNCs also exhibit superior fracture toughness ( $K_{IC} = 15 \text{ MPa m}^{1/2}$ ) and wear resistance ( $W_H = 11$ ; for comparison,  $W_H = 3\text{--}4$  for industrial polycrystalline diamond) and excellent thermal stability (beyond 1600 K in air), making them a potential superabrasive candidate. Higher pressures can supply adequate driving force for hBN-to-cBN transformation that is conducive to the nucleation of cBN, and decelerate the diffusional grain growth, which results in the formation of smaller grains of cBN and hence the improvement of the hardness owing to the Hall–Petch effect. Following this route, Solozhenko et al. also carried out a series of experiments to synthesize nanocrystalline cBN at higher pressures (up to 20 GPa) and lower temperatures (down to 1500 °C) [45].

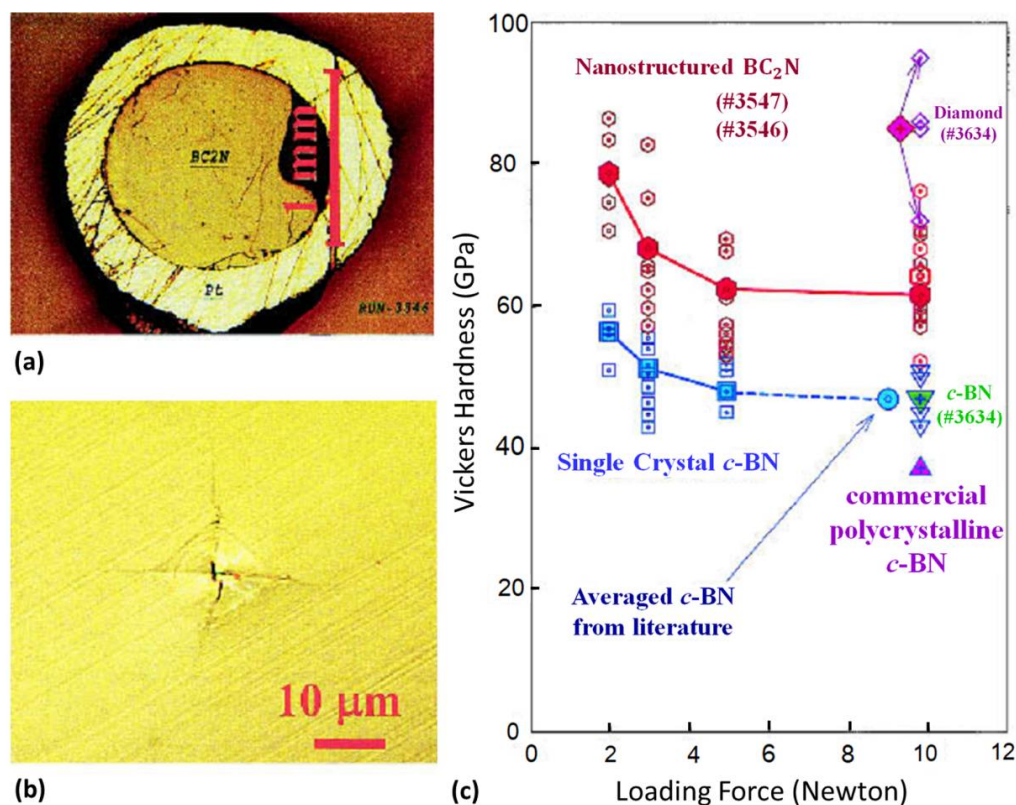


**Figure 3.** (a) Optical micrograph of the BC<sub>2</sub>N sample synthesized under high P–T conditions. The outer yellowish ring is the platinum capsule. (b) Vickers indentation produced by a diamond indenter at a loading force of 9.8 N. (c) Vickers hardness data. Empty symbols show individual measurements, whereas filled symbols are averaged data. For comparison, the figure also shows hardness measurements for cBN single crystals, polycrystalline diamond, and cBN composite (run no. 3634). The circle denotes the average hardness of cBN at a loading force of 9.8 N taken from the literature. The empty inverted triangles show the measurement on cBN from the diamond + cBN composite, and the filled inverted triangle shows the average of the measurements. These measured data agree exactly with the highest hardness to date on the well-sintered polycrystalline cBN sample. The upright triangle denotes the hardness of currently available commercial polycrystalline cBN (Valenite Polycrystalline Products). The empty diamond symbols show the measurement on diamond from the synthesized diamond + cBN composite, and the filled diamond symbol shows the average of the measurements. Reprinted with permission from Zhao et al., *J. Mater. Res.* 17, 3139–3145 (2002). Copyright 2002 Materials Research Society (Ref. [14]).

Figure 4a shows the equation of state of nano-cBN in comparison to that of microcrystalline cBN at room temperature. The obtained bulk modulus of  $B_0 = 375(4)$  GPa approaches the value of 377(4) GPa previously reported for micro crystal cBN. Figure 4b shows the striking dependence of the hardness ( $H_V$ ) on the particle size. The load-dependence of the Vickers hardness for the nano-cBN sample prepared at 20 GPa and 1500 °C is shown in inset of Figure 4b. The hardness of nano-cBN with a grain size of 20 nm ( $H_V = 85(3)$  GPa) nearly doubles that of conventional microcrystalline cBN ( $H_V \sim 40$ –50 GPa) owing to the size effect. The fracture toughness of nano-cBN ( $K_{Ic} = 10.5$  MPa m<sup>1/2</sup>) is also much higher than those of all known superhard phases in the B–C–N system (5.3 MPa m<sup>1/2</sup> for both single-crystal and polycrystalline diamond; 2.8 and 6.8 MPa m<sup>1/2</sup> for single-crystal and micrometer-sized cBN, respectively; and 4.5 MPa m<sup>1/2</sup> for nanocrystalline cubic BC<sub>2</sub>N).<sup>13,45</sup> Nano-cBN has outstanding chemical stability; the onset temperature of oxidation in air,  $T_{ox}$ , is 1460 K for nano-cBN, significantly higher than those of microcrystalline ( $T_{ox} \sim 1100$  K) and nanocrystalline diamond ( $T_{ox} \sim 950$  K for the grain-size of 10–15 nm), and comparable with that of microcrystalline cBN ( $T_{ox} \sim 1520$  K) [8,13,45].

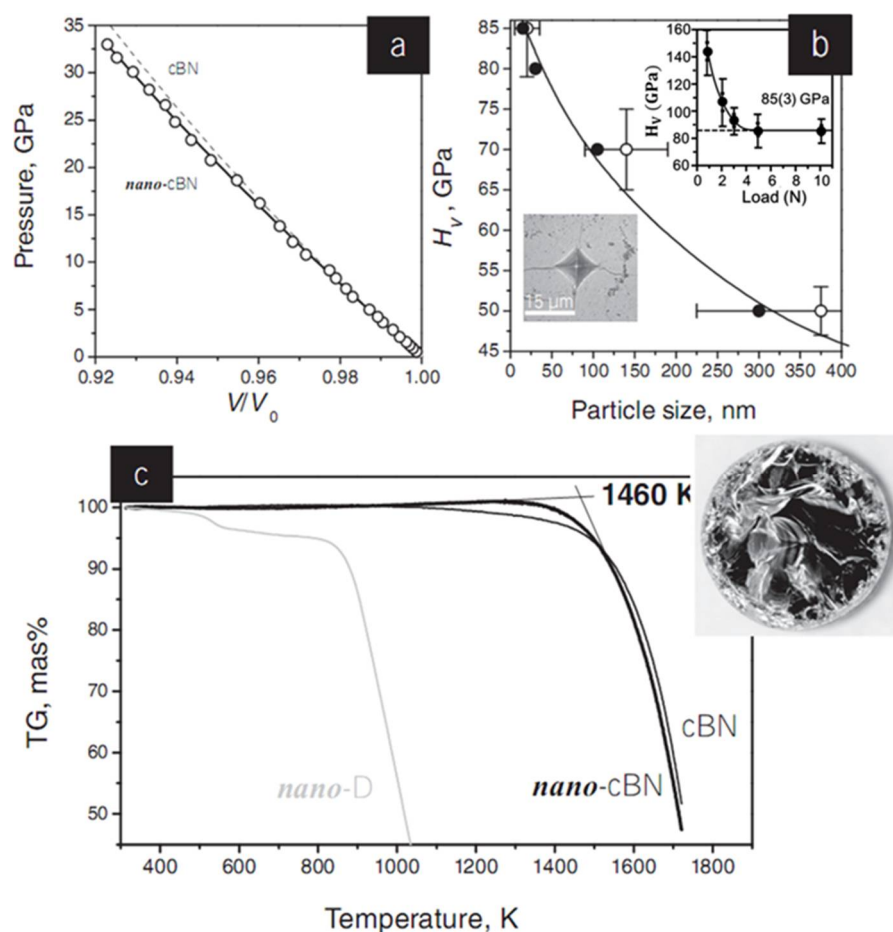


**Figure 4.** Properties of a nano-cBN sample obtained from pBN at 20 GPa and 1770 K. (a) 300 K equation of state data for nano-cBN up to 35 GPa. The circles represent experimental points, while the solid line shows the fit of experimental data to the Vinet equation of state with bulk modulus of  $B_0 = 375(4)$  GPa and its pressure derivative of  $B'_0 = 2.3(3)$ . Equation of state of micrometer-sized cBN (dashed line) is given for comparison. (b) Dependence of the Vickers hardness on cBN grain size evaluated from X-ray diffraction (solid circles) and ATEM (open circles) data. This dependence follows the Hall–Petch relationship and results from the nanosize effect, which restricts dislocation propagation through the material. Top inset: Vickers hardness as a function of applied force. The calculated hardness drops from  $\sim 150$  GPa (at 1 N) down to its asymptotic value of  $85(3)$  GPa (above 5 N). Bottom inset: Optical microscope image of the Vickers indentation with cracks. (c) Thermogravimetric data (in air) for nano-cBN (the onset temperature of oxidation  $T_{ox}$  is 1460 K), nanocrystalline (10–15 nm) diamond ( $T_{ox} \sim 950$  K), and microcrystalline cBN ( $T_{ox} \sim 1520$  K). Inset: Optical microscope image of the nano-cBN bulk. Reprinted with permission from Solozhenko et al., *Adv. Mater.* 24, 1540–1544 (2012). Copyright 2012 John Wiley and Sons, Inc. (Ref. [45]).

Tian et al. synthesized at high- $P$  and high- $T$  nano-twinned cBN with an average thickness of 3.8 nm using an onion-like BN precursor that possesses nested structures with constitutionally puckered BN layers and plenty of stacking-faults [7]. The optically transparent nano-twinned cBN bulk sample has a greatly high Vickers hardness (beyond 100 GPa, the optimal hardness of man-made diamond), a superior oxidation temperature (1294 °C), and an advanced fracture toughness ( $12 \text{ MPa m}^{1/2}$ , well exceeding the toughness of commercial cemented tungsten carbide(WC),  $10 \text{ MPa m}^{1/2}$ ) [7].

Figure 5a,b shows the starting oBN nanoparticles ( $\sim 30$ – $150$  nm in diameter) forming concentric cBN round shells with plentiful puckering and stacking-faults. The transparent cBN (Figure 5c) was synthesized above 1600 °C at 15 GPa. Figure 5d–f show the typical TEM and HRTEM photographs of a bulk nano-twinned cBN sample, which has a similar

grain size as the original onions. HRTEM revealed high density of dislocations between grain-boundaries and high-density of stacking-faults in the twin regions. Figure 5e,f exhibits narrow and sharp high-angle grain boundaries about five or six atomic layers thick (below 10 nm, with an average of 3.8 nm). Surprisingly, the bulk nano-twinned cBN sample has obtained an asymptotic hardness value of  $\sim 108$  GPa at loads of 3 Newtons and more via standard square-pyramidal diamond indentation measurements (see Figure 6), which transcends the hardness of the hardest polycrystalline cBN reported so far ( $\sim 85$  GPa), and even that of synthetic diamond ( $\sim 100$  GPa). The quantum confinement effect dominates the hardening mechanism when nano-twins are less than 3.8 nm thick. Twin dislocations severely limit the migration of twin boundaries, which is responsible for the extreme hardness of nano-twinned cBN.

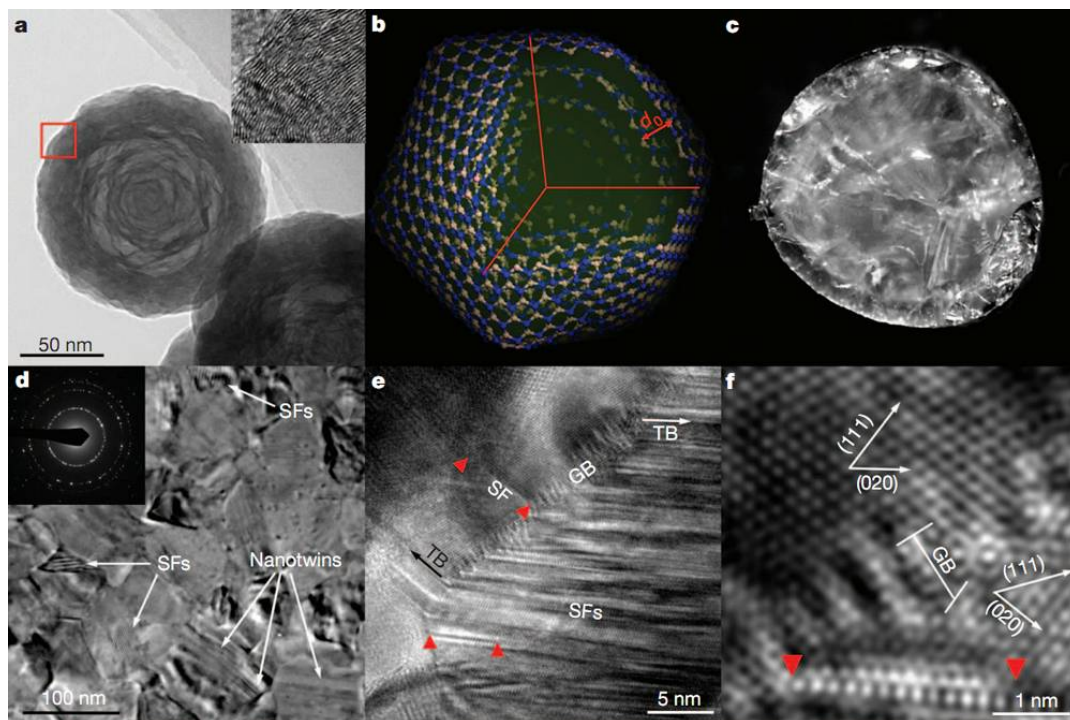


**Figure 5.** Starting oBN nanoparticles and nt-cBN bulk synthesized at 15 GPa and 1800 °C. (a) TEM image of oBN nanoparticles. Inset, HRTEM image corresponding to the position marked with the red box, showing defects including lattice puckering, bending, and stacking faults. (b) Schematic icosahedral model of a five-shell oBN nanoparticle.  $d_0$  is the inter-shell spacing. (c) Photograph of an nt-cBN bulk sample with a diameter of about 2 mm. (d) TEM image of a typical microstructure in nt-cBN. Nanotwins and stacking faults (SFs) are marked. Inset, a selected area electron diffraction pattern. (e) HRTEM image of nt-cBN showing Shockley partial dislocations (red triangles) emitted from grain boundaries (GB) and a high density of stacking faults in twin domains. TB, twin boundary. (f), Enlarged HRTEM image of e, showing the orientation relationship between adjacent nanograins. Reprinted with permission from Tian et al., Nature 493, 385 (2013). Copyright 2013 Nature Publishing Group (Ref. [7]).

Recently, Liu et al. have reported the sintering of sm-cBN at a relatively low pressure of 8 GPa [32]. These sm-cBN bulks exhibit a hardness comparable to that of single-crystal diamond and a fracture toughness ( $13.2 \text{ MPa m}^{1/2}$ ) 5 times as much as that of single-crystal cBN ( $2.8 \text{ MPa m}^{1/2}$ ), as well as excellent chemical stability. In comparison to other ultrahard materials, the sm-cBN aggregates have potential industrial application because their relatively low preparation pressure makes large-scale production possible, and hence reduces the fabricating costs.

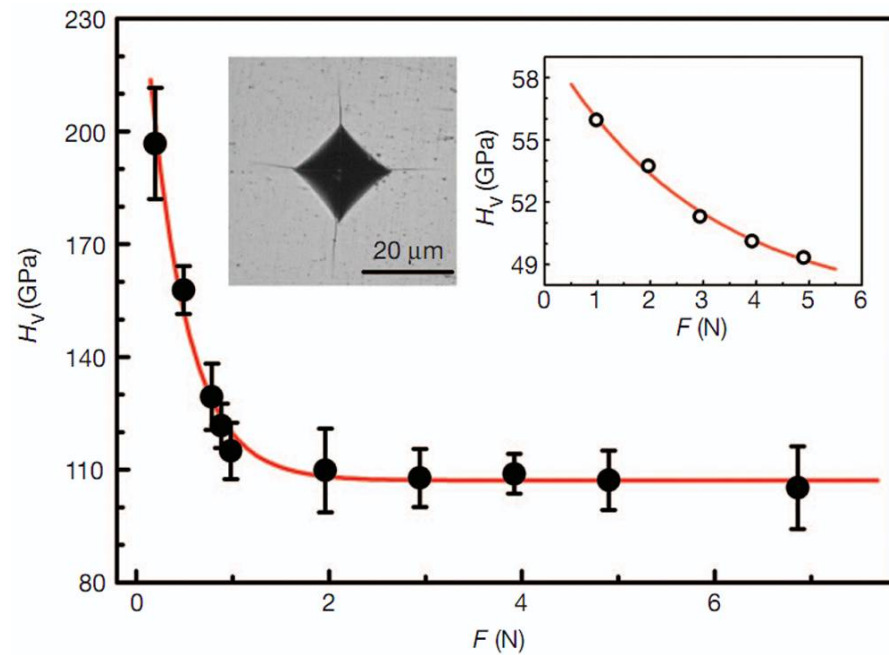


**Figure 6.** The  $H_V$  of an nt-cBN bulk sample as a function of applied load ( $F$ ). The  $H_V$  of the nt-cBN bulk decreases from  $\sim 196$  GPa at 0.2 N to its asymptotic value, 108 GPa, beyond 3 N. Error bars indicate s.d. ( $n = 5$ ). Left inset, an optical micrograph of the Vickers indentation with cracks produced at a load of 19.6 N. Right inset, the  $H_V$ - $F$  curve of a 0.3 mm cBN single crystal.  $H_V$  does not reach its asymptotic value, and the crystal fractures when  $F$  exceeds 4.9 N. Reprinted with permission from Tian et al., Nature 493, 385 (2013). Copyright 2013 Nature Publishing Group (Ref. [7]).

As shown in Figure 7a, the Vickers hardness for the sm-cBN compacts sintered at 8 GPa and 2300 K is  $112 (\pm 3)$  GPa at the load of 2.94 N, which is higher than that of nano-twinned cBN ( $\sim 108$  GPa) at the same loading<sup>7</sup> and has been claimed to be the highest hardness reported heretofore for polycrystalline cBN. An asymptotic hardness of  $75 (\pm 3)$  GPa was reached at loading force above 29.4 N, which is quite higher than that of single-crystal cBN ( $\sim 50$  GPa) and comparable with that of single-crystal diamond (60–120 GPa). Moreover, the sm-cBN aggregates also have good thermal stability; onset oxidation temperature ( $1255^\circ\text{C}$  in air) is significantly higher than that of single-crystal ( $\sim 1106^\circ\text{C}$ ) and nano-grained cBN ( $\sim 1190^\circ\text{C}$ ) (inset of Figure 7b). The sm-cBN samples were tested via high-speed cutting of hardened steel (hardness  $HRC = 62$ , cutting speed: 120 m/min, feed: 0.15 mm/rev, and depth of cut: 0.1 mm) and compared with the performance of commercial PcBN. As shown in Figure 7c, the sample synthesized at 8 GPa and  $2000^\circ\text{C}$  had less flank wear ( $V_b$ ) than commercial cBN at the same cutting time, especially at longer duration, meaning sm-cBN has a better wear resistance.

Carbon-carbon (C-C) bonds in diamond break down at a relatively low temperature during oxidation and are the culprit for its poor chemical stability. Because of the chemical inertness of B-C and C-N bonds, it is conceivable that forming B-C-N solid solutions in the out layers of a diamond grain could protect C-C bonds from oxidation, hence improving their chemical stability. Meanwhile, the core diamond would retain much of the hardness, resulting in a composite with various desired properties. We have successfully synthesized transparent bulk diamond-cBN alloy compacts at high pressure and temperature (Figure 8) [12]. The analytic results revealed that the diamond-cBN alloy has significantly better chemical inertness than pure polycrystalline diamond and is harder than single-crystal cBN. High-speed dry cutting tests on hardened steel and granite indicated the diamond-cBN alloy is indeed a universal cutting material.

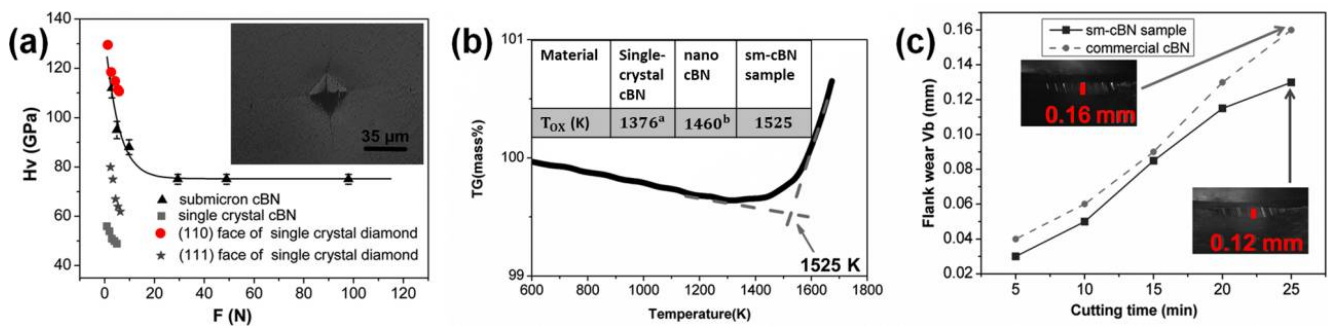


**Figure 7.** Properties of a sample sintered at 8 GPa and 2300 K. (a) Vickers hardness as a function of applied load force. Inset: an optical micrograph of the Vickers indentation with cracks produced at a load of 49 N. For single-crystal cBN, the value of Vickers hardness is ~50 GPa; for the single-crystal diamond, the values of Vickers hardness are ~110 GPa on the {1 1 0} face and ~62 GPa on the {1 1 1} face. (b) The thermogravimetric curve for sm-cBN sample. Inset: table showing oxidation temperatures of different cBN samples. (c) The width of wear on the as-prepared sm-cBN sample and commercial cBN as functions of cutting time. Inset: photographs of the sm-cBN samples at a cutting time of 25 min. Reproduced from Guoduan Liu, Zili Kou, Xiaozhi Yan, Li Lei, Fang Peng, Qiming Wang, Kaixue Wang, Pei Wang, Liang Li, Yong Li, Wentao Li, Yonghua Wang, Yan Bi, Yang Leng, and Duanwei He. “Submicron cubic boron nitride as hard as diamond.” *Appl. Phys. Lett.* 106, 121901 (2015), with the permission of AIP Publishing.

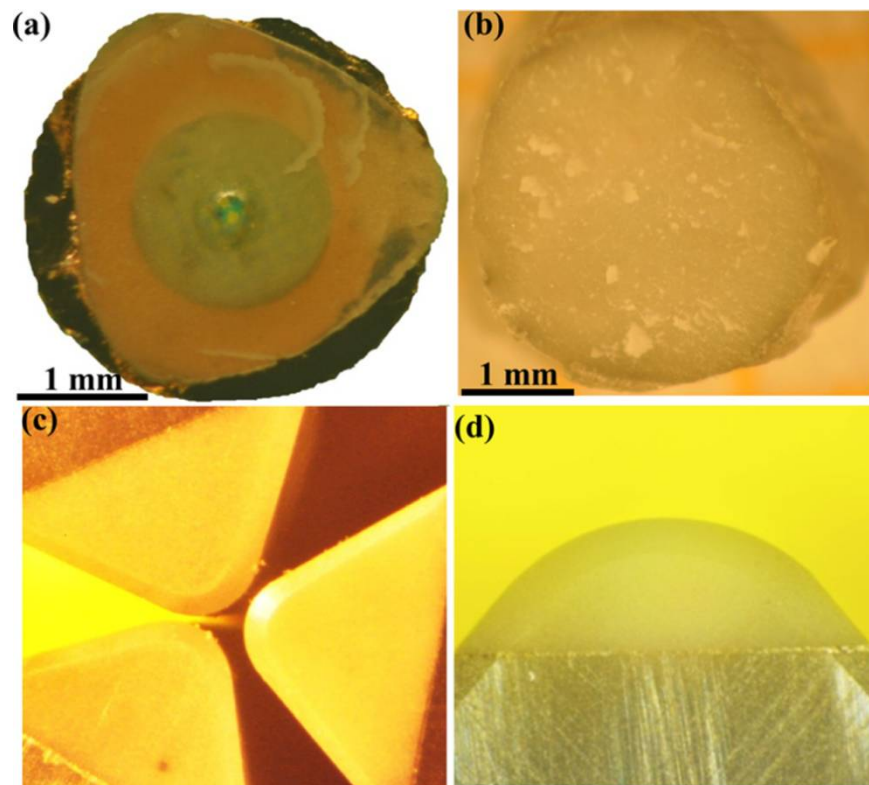


**Figure 8.** Photographs of diamond-cBN bulk samples and diamond-cBN alloy cutters. (a) and (b) Bulk diamond-cBN alloy samples synthesized at 20 GPa/2500 K with a diameter of ~3 mm, over a copper screen to exhibit its transparency. (c) and (d) Polished rake faces of diamond-cBN alloy cutters. Reproduced from Wang et al. “Diamond-cBN alloy: A universal cutting material.” *Appl. Phys. Lett.* 107, 101901 (2015), with the permission of AIP Publishing.

The diamond–cBN alloy bulk sample synthesized at 19 GPa/2000 °C has a Vickers hardness of  $78 \pm 5$  GPa under a load force of 9.8 Newtons, a value close to the hardness of single-crystal diamond ( $H_V$ : 60–120 GPa) and far exceeding the hardness of single-crystal cBN ( $H_V \sim 50$  GPa) [12,14]. The onset oxidation-temperature for diamond–cBN alloys (1070 K) is more upper than that of PCD (869 K) but more inferior than that of cBN (1343 K). X-ray photoelectron spectroscopic (XPS) measurements confirmed new B–C and C–N bonds in diamond–cBN alloys that are presumably produced at or near diamond–cBN grain boundaries.

High-speed cutting test on hardened steel ( $HRC \sim 62$ ) (cutting speed  $\sim 120$  mm/min, feed  $\sim 0.1$  mm/rev, and depth of cut  $\sim 0.1$  mm) indicated diamond–cBN alloy rivals the commercial PcBN in terms of wear resistance and tool life, and both are much better than PCD in these regards (Figure 9a,b). Compared to commercial PCD and PcBN, diamond–cBN alloy has again the best property with uniformly less average flank face wear when tested on granites, resulting in the longest tool life among the three materials (Figure 9c,d).

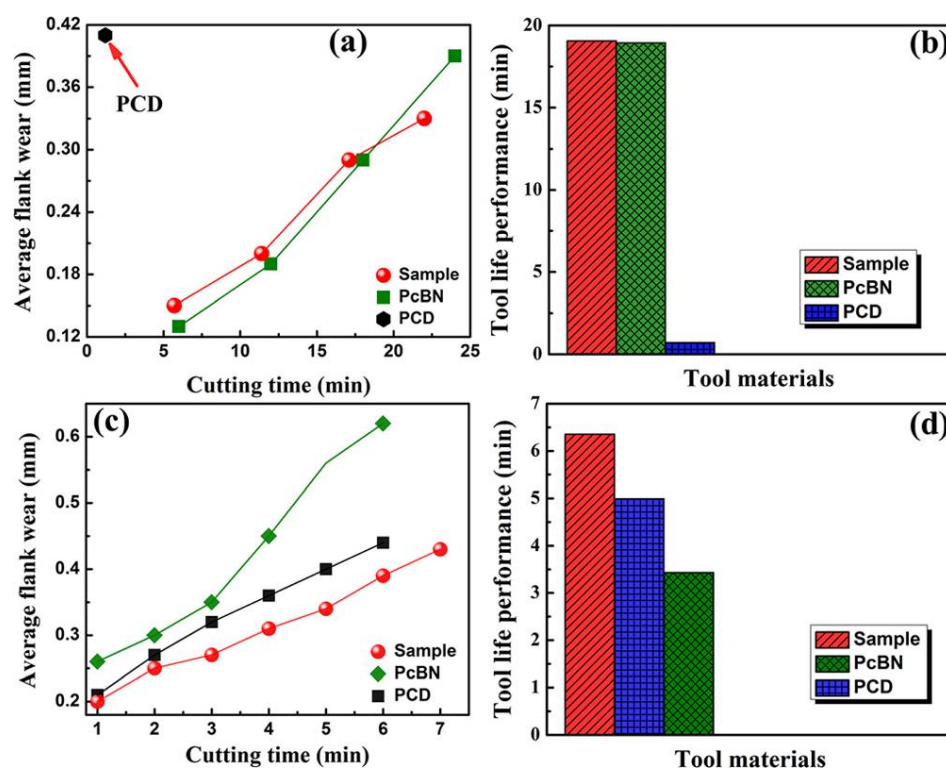


**Figure 9.** The cutting performance of diamond–cBN alloy compared to commercial PcBN and PCD. (a) and (c) Average flank wear versus time (min) for diamond–cBN alloy, PCD, and PcBN tools during dry cutting of hardened steel and granite. (b) and (d) Tool life performance for diamond–cBN alloy, PCD, and PcBN tools during dry cutting of hardened steel and granite. Reproduced from Wang et al. “Diamond–cBN alloy: A universal cutting material.” *Appl. Phys. Lett.* 107, 101901 (2015), with the permission of AIP Publishing.

#### 4. Preparation of Transition Metal Nitride Alloys: Challenges and Opportunities

TMNAs in recent years have drawn significant attention due to their fundamental and technological importance [41–44,71–76]. They are characterized by strong covalent bonds between nitrogen atoms and polar covalent bonds between transition-metal and nitrogen atoms. As such, TMNAs are usually hard or potentially superhard materials with outstanding chemical inertness. For example, as a group of classical hard materials, transition-metal mononitrides, such as TiN, CrN, WN, HfN, and ZrN, are used as coating or covering layers for cutting tools to process ferrous alloys because of their remarkable stability [41–44,71–76]. Some TMNAs are superconductors [33], and some possess unusual magnetic properties [77], making them good candidate materials for un-

raveling fundamental physics. However, it is challenging to synthesize TMNAs through conventional methods because the incorporation of nitrogen into the transition metal lattice is thermodynamically unfavorable in an ambient condition, which usually results in low-crystallinity, low-nitrogen content, and nonstoichiometric products, leading to the difficulties and ambiguities in determining various critical properties of TMNAs. Extensive experimental studies have been focused on the preparation of stoichiometric TMNAs with nitrogen-to-metal ratio greater than unity and of high-crystallinity.

Lei et al. developed an effective preparation method for well-crystallized gallium nitride (GaN) via an unconventional solid-state metathesis (SSM) reaction at high-pressure between varying phases of lithium metagallate ( $\text{LiGaO}_2$ ) and hBN [40,78]. Subsequently, Wang et al. employed this method and successfully synthesized a series of hard metal nitride alloys using ion-exchange reactions under moderate pressure and temperature [41–44]. For instance, well-crystallized bulk and stoichiometric CrN crystals have been synthesized via solid-state ion-exchange between  $\text{Na}_2\text{CrO}_4$  and hBN [42]. Figure 10 exhibits typical scanning electron microscope (SEM) images of euhedral CrN crystals with a relatively uniform crystal-size. Moreover, they have also found that the solid-state ion-exchange at moderate pressure is more time-efficient (only 20 min needed to grow 1  $\mu\text{m}$  CrN crystals at 3–5 GPa and 1200  $^\circ\text{C}$ ) than the traditional ammonolysis of  $\text{Cr}_2\text{S}_3$  (heating time in excess of 12 h at 800–1000  $^\circ\text{C}$ ) [79]. In addition, the former method can prepare high-crystallinity and nitrogen-rich metal nitride alloys, while the latter method usually resulted in poorly crystallized products with a flocculent shape.

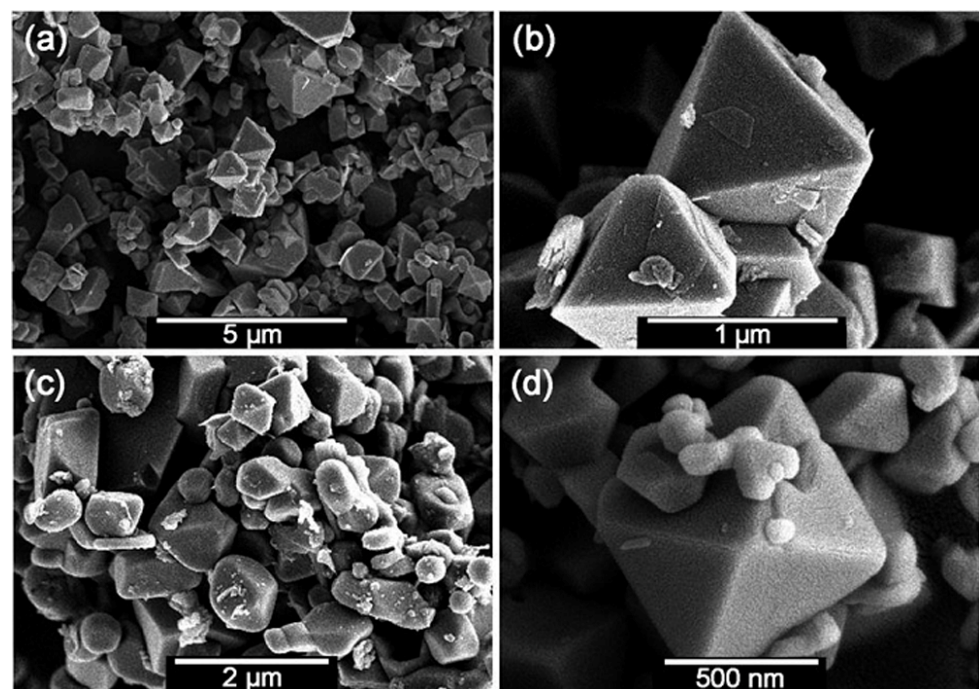


**Figure 10.** Typical SEM images for CrN crystals prepared at 5 GPa and 1200  $^\circ\text{C}$  for 20 min (a) with an enlarged fragment shown in (b), at 3 GPa and 1200  $^\circ\text{C}$  for 20 min (c), and at atmospheric pressure and 1000  $^\circ\text{C}$  for 2 h in Ar gas (d). Reprinted with permission from Chen et al., Chem.: Eur. J. 18, 15459–15463 (2012). Copyright 2012 John Wiley and Sons, Inc. (Ref. [12]).

Lei and Wang et al. have continuously improved the solid-state ion-exchange method and devoted more efforts to synthesizing TMNAs at high pressure. A series of TMNAs with high-crystallinity, such as hexagonal nitrides  $\text{W}_2\text{N}_3$ , WN,  $\delta$ -MoN,  $\text{Fe}_3\text{N}$ , and  $\text{Re}_3\text{N}$ , and cubic nitrides  $\text{W}_3\text{N}_4$  (see Figure 11),  $\gamma$ -MoN, and VN, have also been synthesized via the same method using metal salts and hBN [40–44,78,80,81]. Recently, Wang et al. have synthesized the hardest superconducting transition-metal nitride cubic  $\gamma$ -MoN and hexagonal  $\delta$ -MoN with an asymptotic Vickers hardness of  $\sim 23$  and  $\sim 30$  GPa [33,44], respectively,

as shown in Figure 12a–c. The hardness of  $\delta$ -MoN exceeds that of commercial cemented tungsten carbide (WC  $\sim$  20 GPa) [21] and moissanite (SiC  $\sim$  22 GPa) [82] and approaches that of one of the hardest transition metal borides  $WB_4$ . Hexagonal  $\delta$ -MoN, which is  $\sim$ 9.5% less dense than the  $\gamma$  phase, is supposed to be less resistant to external shear and compression, i.e., to have lower hardness; however,  $\delta$ -MoN deviates from this trend and stands out to be the hardest metal nitride, as shown in Figure 12d–f. The strong 3D anion–cation bonding networks in  $\delta$ -MoN are responsible for its abnormally high hardness. All results above indicate that the novel approach involving ion-exchange reactions under moderate pressures and temperatures is a shortcut for rapidly synthesizing high-crystallinity, stoichiometric, and nitrogen-rich TMNAs. The availability of such high-quality specimens will indeed help open many new windows in this exciting emergent subfield of materials research.

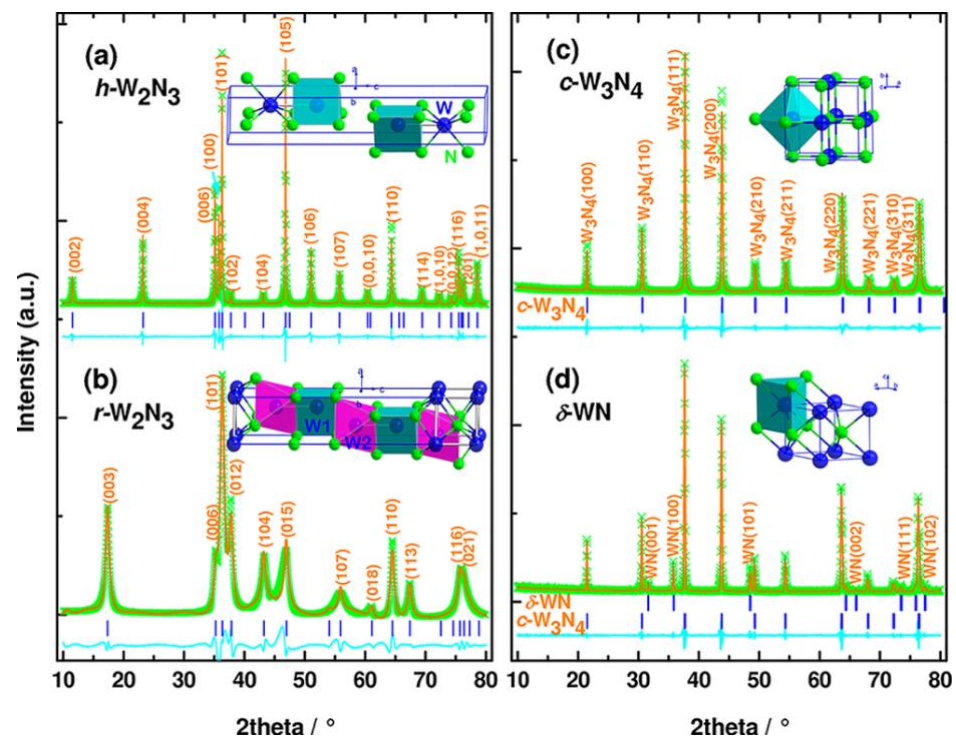


**Figure 11.** XRD patterns of nitrides in the binary system W–N. The observed (green crosses) and calculated (solid orange lines) profiles for  $h$ - $W_2N_3$  (a) and  $r$ - $W_2N_3$  (b), synthesized at 5 GPa and temperatures of 1480 and 880 K, respectively, and purified by removing by-product  $NaBO_2$  (see Experimental Section);  $c$ - $W_3N_4$  (c) and  $\delta$ -WN (d), prepared from  $h$ - $W_2N_3$  at 5 GPa and 2273 and 2570 K, respectively. The curves in the cyan color represent the difference between the observed and calculated profiles. Insets are crystal structures of those nitrides. The blue tick marks correspond to the peak positions. Reprinted with permission from Wang et al. “Synthesis, Crystal Structure, and Elastic Properties of Novel Tungsten.” *Chem. Mater.* 24, 3023–3028 (2012), Copyright 2012 American Chemical Society. (Ref. [41]).

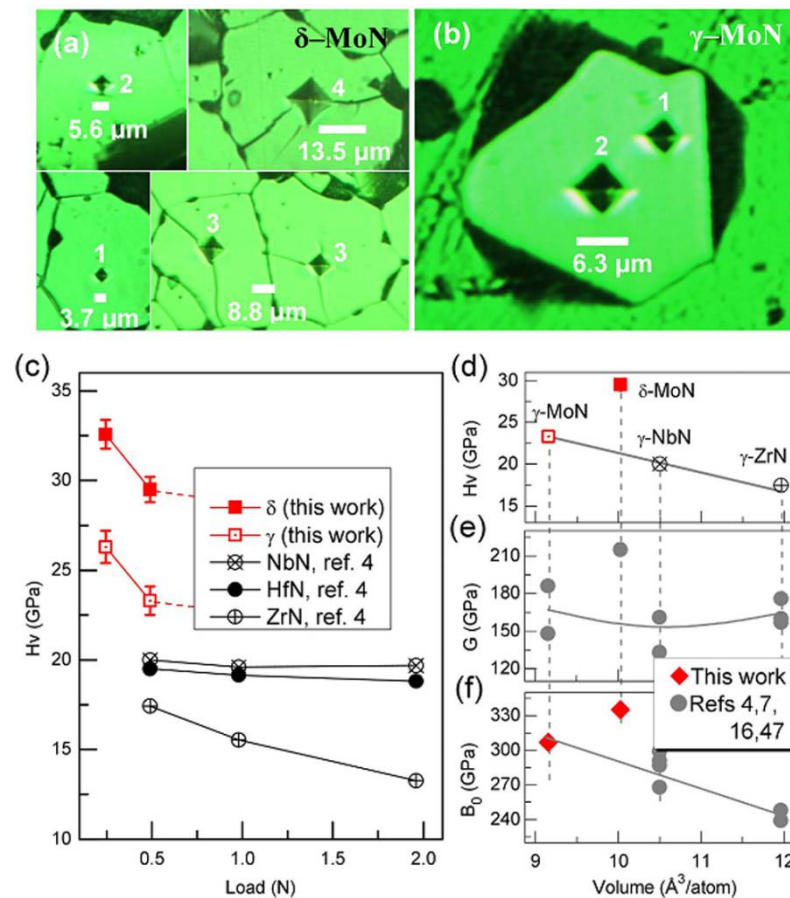


**Figure 12.** (a,b) Vickers hardness measurement for single-crystal  $\delta$ - and  $\gamma$ -MoN. Indentations numbered with '1', '2', '3', and '4' correspond to applied loads of 0.245, 0.49, 0.98, and 1.96 N, respectively. The crystals in (a) were prepared by sintering of phase-pure  $\delta$ -MoN powders at 8 GPa and 1800 °C for 60 min. The  $\gamma$ -MoN crystal in (b) was directly grown using an ion-exchange reaction (see Figure 1e). (c) Vickers hardness,  $H_V$ , of  $\delta$ - and  $\gamma$ -MoN as a function of applied load. Also plotted are the reported  $H_V$  values for other hard nitrides including ZrN, NbN, and HfN (ref. [4]). (d)  $H_V$  vs. volume per atom (i.e., normalized volume in terms of per atom) for  $\gamma$ -MoN,  $\gamma$ -ZrN (ref. [4]), and  $\gamma$ -NbN (ref. [4]) under a load of 0.49 N. (e) Bulk modulus,  $B_0$ , vs volume per atom. The measured bulk moduli for  $\delta$ - and  $\gamma$ -MoN are  $\sim$ 335 and  $\sim$ 307 GPa, respectively, based on compression experiments (Suppl Figures S6 and S7). (f) Shear modulus,  $G$ , vs. volume per atom. Reprinted with permission from Wang et al., "The hardest superconducting metal nitride." *Sci. Rep.* 5, 13733 (2015), Copyright 2015 Nature Publishing Group. (Ref. [33]).

## 5. Discussions

Based on previous experimental studies on the mechanical properties of nitrides, hardness, which is a weighted sum of intrinsic and extrinsic hardening effects and factors, is the most important performance index empirically correlated with shear modulus ( $G$ ) or ratio of  $G/B$  of materials,  $B$  is bulk modulus, as shown in Figure 13a,b. It is apparent that most light-element nitride materials have higher  $G$  or ratio of  $G/B$  than those of metal nitrides due to their short and strong covalent bonding and 3-D network crystal-structure, leading to their overall robust resistance to compression and shear deformation [6,83] and hence their high hardness. However, experimental observation on the indentation processes during the hardness measurement is largely lacking. Deeper understanding of deformational mechanisms at high pressure may be key to designing new superhard materials. To synthesize nitride materials suitable for machining ferrous metals, more efforts are needed to focus on synthesizing ternary or multi-component solid-solutions in B-C-N, B-O-N, Si-C-N, or B-C-N-O systems using the high-pressure method. Light elements, such as Si,

B, C, and O, as solute atoms incorporated in nitrides can introduce the local nonuniformity in the lattice, resulting in superior strength for nitride materials. Moreover, mechanical properties of bulk light-element nitrides can be further improved through microstructure manipulations, such as the formation of pressure-induced nano-twins and high-density dislocations [3,4,7–9,32,46,47,69,70,84–87]. Both methods can lead to significant hardening of bulk nitrides by impeding the motion of dislocation. However, synthesis of these superhard nitride materials generally needs extreme pressure and temperature. To prepare bulk samples, which requires the experimental apparatus to not only produce ultrahigh pressure ( $\geq 15$  GPa) and high temperature ( $\geq 2000$  °C) [3,4,7,8,12,14,53–57] but also possess a large sample chamber (at mm scale), current static high-pressure multi-anvil technology needs to be improved. Thus, the design and preparation of novel superhard nitride materials simultaneously possessing outstanding mechanical performance and high chemical inertness, as well as meeting the sample-size requirement for practical industrial application, is one of the most challenging research subjects due to high cost and technical difficulties in ultrahigh pressure generation. Fortunately, bulk superhard materials synthesized via high-pressure and high-temperature can in turn be used to improve pressure-generation technology. For instance, synthetic bulk NPD as anvils have been used to generate high pressure up to 120 GPa while maintaining the sample chamber at mm-scale [87]. Synthetic PCD, PcBN, sm-cBN, nano-twinned diamond and cBN, and B–C–N materials are also anvil candidates for generating ultrahigh pressures at large sample volumes.

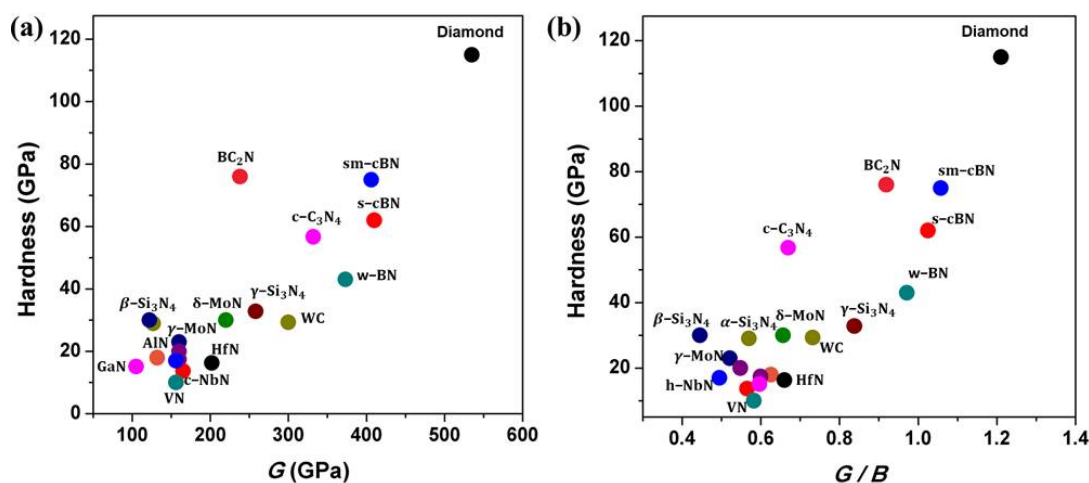


**Figure 13.** Correlation of experimental hardness for diamond, tungsten carbide, and some nitrides with (a) the shear modulus,  $G$ , and (b)  $G/B$ , where  $B$  is the bulk modulus, for 21 compounds (see Table 1); moduli of cubic  $C_3N_4$  and wurtzite boron nitride (w-BN) are from theoretical calculations.

As mentioned above, cost and efficiency need to be considered for industrial application of nitride materials besides their excellent mechanical performances. Large-scale industrial production and significant market penetration ask for synthesis conditions for nitride materials of moderate pressures and temperatures. Ion-exchange reactions are a shortcut for rapidly synthesizing high-crystallinity, stoichiometric, and nitrogen-rich TMNAs under moderate conditions. Meanwhile, novel ternary TMNAs, such as  $Zn_3WN_4$ ,  $Mg_2NbN_3$ , and  $MgTiN_2$  [88], have just been successfully synthesized via magnetron sputtering or soft solid-state synthesis routes. From a broader perspective, these synthesis methods of new ternary nitride alloys provide chemists a new pathway in their quest to continuously extend the frontier of nitride alloys, as shown in Figure 14. Following this advance, more efforts are now needed toward the synthesis of hard or even superhard ternary transition-metal nitrides, such as Ti–C–N, W–Re–N, and Mo–W–N compounds, using high-pressure methods to incorporate suitable solute atoms in parent nitrides. The solute atoms, which can determine the dislocation patterns within nitrides, create local stress fields and again impede the motion of dislocation, resulting in an increase in the yield

stress of the nitrides. In order to achieve noticeable strengthening, solutes of higher shear modulus should be chosen for alloying to increase the local  $G$  and hence stiffness of the nitrides. In addition, alloying elements of different ionic sizes in nitrides can generate local stress. The greater the difference in ionic size, the higher the local stress fields introduced by alloying.

**Table 1.** Elastic properties, hardness, fracture toughness (FT), and thermal stability of diamond, tungsten carbide (WC), and hard or superhard nitride materials: bulk modulus  $B$ , shear modulus  $G$ , ABBNs (aggregated boron nitride nanocomposites), cubic (c) phase, hexagonal (h) phase, single-crystal diamond (S-dia).

Material	Methods	$B$ (GPa)	$G$ (GPa)	$H_V$ (GPa)	FT (MPa m <sup>1/2</sup> )	$T_{ox}$ (°C)	References
S-diamond	Exp.	442	535	115	5	677	[8,13,45,57,89]
S-cBN	Exp.	400	410	67	2.8	1103	[8,13,45,57,90]
nt-cBN	Exp.	–	–	108	5	1294	[7]
nano-cBN	Exp.	375	–	85(3)	10.5	1187	[45]
ABNNC <sub>s</sub>	Exp.	–	–	85(5)	15	1327	[8]
sm-cBN	Exp.	384	406	75(3)	13.2	1252	[32]
w-cBN	Exp.	–	–	43(3)	–	920	[91]
c-C <sub>3</sub> N <sub>4</sub>	Cal.	496	332	87.1	–	–	[17,92]
β-C <sub>3</sub> N <sub>4</sub>	Cal.	437	320	60.4	–	–	[17,92]
CN <sub>x</sub> films	Exp.	–	–	60	–	–	[9,27]
α-Si <sub>3</sub> N <sub>4</sub>	Exp.	223	127	29	–	–	[28,29]
β-Si <sub>3</sub> N <sub>4</sub>	Exp.	274	112	20	3.5	–	[28,29,93]
γ-Si <sub>3</sub> N <sub>4</sub>	Exp.	308	–	30–43	–	–	[28,29]
Dia-Si <sub>3</sub> N <sub>4</sub>	Exp.	–	–	41	–	–	[55]
α-Ge <sub>3</sub> N <sub>4</sub>	Exp.	178	–	–	–	–	[94]
β-Ge <sub>3</sub> N <sub>4</sub>	Exp.	218	–	–	–	–	[94]
γ-Ge <sub>3</sub> N <sub>4</sub>	Exp.	296	–	–	–	–	[94]
B <sub>13</sub> N <sub>2</sub>	Exp.	200	–	–	–	–	[26]
BC <sub>2</sub> N	Exp.	259	238	76(4)	4.5	–	[13,45,57]
BC <sub>2</sub> N	Exp.	276	–	62	–	–	[14,95]
BC <sub>4</sub> N	Exp.	–	–	68	–	–	[14]
Dia-cBN	Exp.	–	–	74	–	797	[12]
δ-MoN	Exp.	335	330	30	–	–	[33,96]
γ-MoN	Exp.	307	160	23	–	–	[33,96]
ReN <sub>2</sub>	Exp.	428	–	–	–	–	[97]
Re <sub>2</sub> N	Exp.	401	–	–	–	–	[98]
Re <sub>3</sub> N	Exp.	395	–	–	–	–	[98]
h-W <sub>2</sub> N <sub>3</sub>	Exp.	331	–	–	–	–	[41]
γ-W <sub>2</sub> N <sub>3</sub>	Exp.	226	–	–	–	–	[41]
c-W <sub>2</sub> N <sub>3</sub>	Exp.	376	–	–	–	–	[41]
AlN	Exp.	132	211	18	–	–	[83,99,100]
ZrN	Exp.	267	160	17.4	–	–	[68,101]
TiN	Exp.	292	160	20(2)	–	–	[68,83,99]
h-TaN	Exp.	288	–	22	–	–	[102,103]
HfN	Exp.	306	202	19.5	–	–	[101]
h-NbN	Exp.	373	201	–	–	–	[104]
c-NbN	Exp.	292	165	20	–	–	[101]
IrN <sub>2</sub>	Exp.	428	–	–	–	–	[71]
OsN <sub>2</sub>	Exp.	358	–	–	–	–	[71]
PtN	Exp.	372	–	–	–	–	[73]
PtN <sub>2</sub>	Exp.	347	–	–	–	–	[76]
c-CrN	Exp.	257	–	16	–	650	[44,105]
VN	Exp.	268	156	10	–	–	[44,106]
GaN	Exp.	176	105	12(2)	0.79	–	[99,107]
Pure WC	Exp.	410	300	29.3	8.9	–	[68,108]

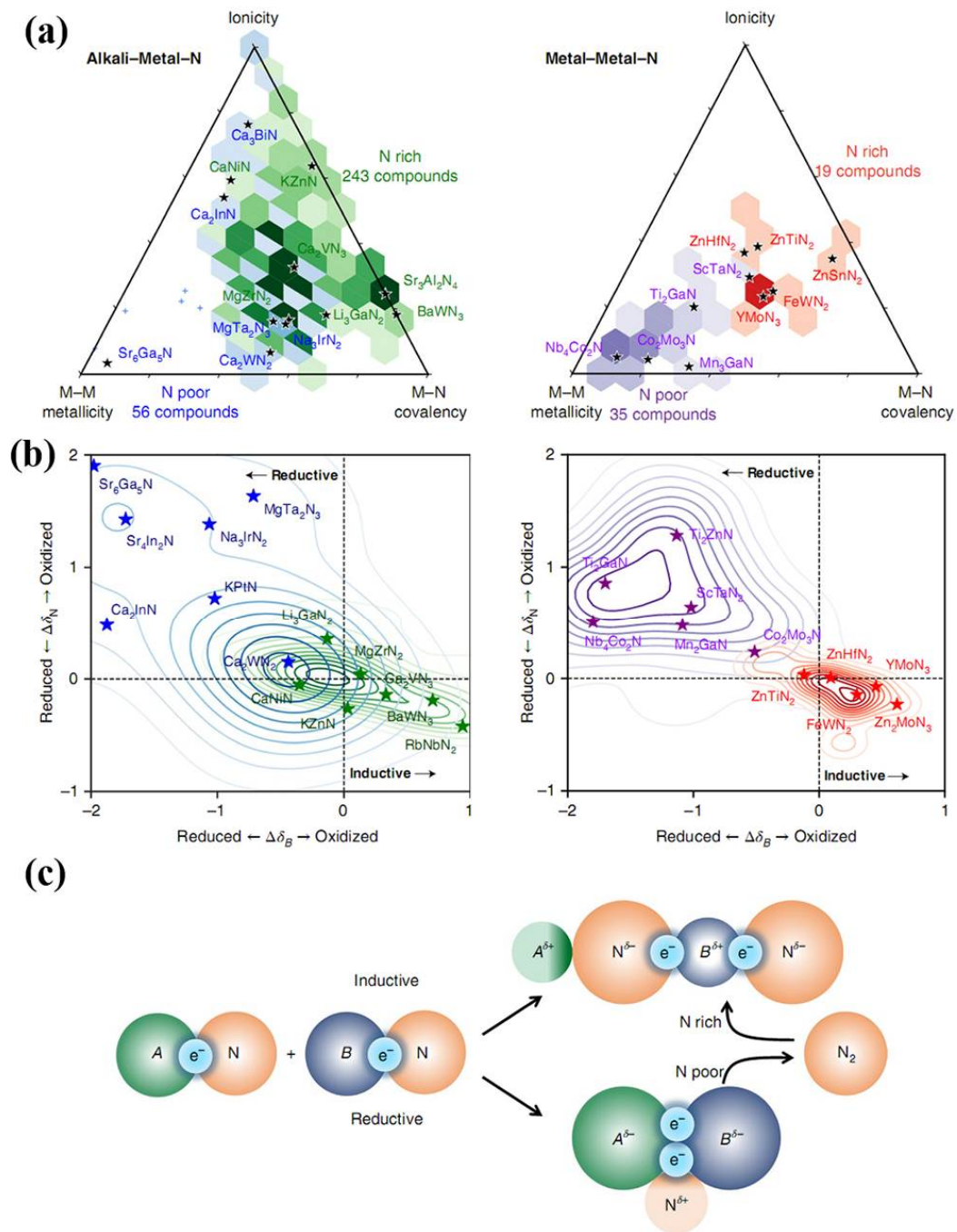


**Figure 14.** Electronic structure origins of ternary nitride stability. (a) Metallicity, ionicity, and covalency of the stable ternary nitrides, hexagonally binned on van Arkel triangles by the nitrogen excess or nitrogen deficiency of the ternary, compositionally referenced against the deepest-hull binary nitrides. Hexagons are plotted for regions with more than two data points only; outliers are shown with small crosses. The color intensity corresponds to the number density in each hexagon. Full van Arkel scatter plots can be found in Supplementary Section 8. (b) Kernel density distributions of ion oxidation and reduction between the deepest-hull binary nitrides and the stable ternary nitride, as determined from the DFT-computed charge density, for the nitrogen anion (vertical axis) and the more electronegative metal, B (horizontal axis). (c) Inductive effect: electropositive metal A donates electron density to the B–N covalent bond, oxidizing the more electronegative metal, which can lead to nitrogen-rich nitrides. Reductive effect: nitrogen oxidation or nitrogen release provides electrons to Me–Me bonds, reducing the metals and increasing metallicity. Reprinted with permission from Sun et al., Nature Materials 18, 732–739 (2019). Copyright 2019 Nature Publishing Group (Ref. [88]).

Compared to light-element nitride materials, TMNAs as cutting tools have many disadvantages, because weaker polar metal–nitrogen covalent bonds or metallic bonds will impair their capabilities of resistance to external shear, which leads to their relatively low hardness. However, similar to conventional metal alloys, TMNAs can be readily manipulated for their microstructures via conventional hardening methods, including cold working, grain-size refinement, second reinforcing phase, and nano-structuring, all of which are effective in forming obstacles to motions of lattice dislocations. More efforts are needed on harvesting work hardening effects using a high-pressure process.

## 6. Conclusions

Synthesis of light-element nitride materials and transition metal nitrides plays a key role in supplementing hard/superhard materials for machining ferrous alloys, as well as providing excellent samples for fundamental research in physics, chemistry, and material sciences. Great strides have been made in this emergent field in recent years. However, due to their relatively low hardness and/or high costs of preparation, the market penetration of nitride materials has so far been limited. Future efforts should be devoted to developing new preparation routines for synthesizing superhard light-element nitride materials at moderate conditions of pressure and temperature. Improving multi-anvil press technologies to increase sample volume at a given pressure will greatly help reduce the costs. Discovering more innovative methods such as ion-exchange reactions under pressures will lead to growing even larger single crystals of transition-metal nitrides. Expanding from single and binary systems to ternary and quaternary systems creates more possibilities in finding new phases of hard/superhard materials. Finally, new microstructural modifications to bulk nitride materials for work hardening are imperative for advancing their industrial applications in machining technology.

**Author Contributions:** P.W., L.W., and Y.Z. (Yusheng Zhao) designed the project. P.W. analyzed the data and wrote the draft. L.W. edited the manuscript. All authors discussed the results and provided inputs for data interpretation. All authors have read and agreed to the published version of the manuscript.

**Acknowledgments:** This work is supported by the National Natural Science Foundation of China (Grant No. 52002166, U2030110 and 11872198), the Shenzhen Development and Reform Commission Foundation for Shenzhen Engineering Research Center for Frontier Materials Synthesis at High Pressures, the Shenzhen Peacock Plan (No. KQTD2016053019134356), the Guangdong Innovative & Entrepreneurial Research Team Program (No. 2016ZT06C279), and the Shenzhen Development and Reform Commission Foundation for Novel Nano-Material Sciences and the Research Platform for Crystal Growth & Thin-Film Preparation at SUSTech.

**Conflicts of Interest:** The authors declare no conflict of interest.

## References

1. Bundy, F.P.; Hall, H.T.; Strong, H.M.; Wentorf, R.H. Man-Made Diamonds. *Nat. Cell Biol.* **1955**, *176*, 51–55. [[CrossRef](#)]
2. McMillan, P.F. New materials from high-pressure experiments. *Nat. Mater.* **2002**, *1*, 19. [[CrossRef](#)] [[PubMed](#)]
3. Huang, Q.; Yu, D.; Xu, B.; Hu, W.; Ma, Y.; Wang, Y.; Zhao, Z.; Wen, B.; He, J.; Liu, Z.; et al. Nanotwinned diamond with unprecedented hardness and stability. *Nature* **2014**, *510*, 250. [[CrossRef](#)]
4. Irifune, T.; Kurio, A.; Sakamoto, S.; Inoue, T.; Sumiya, H. Ultrahard polycrystalline diamond from graphite. *Nature* **2003**, *421*, 599. [[CrossRef](#)] [[PubMed](#)]
5. Wentorf, R.H. Cubic form of boron nitride. *J. Chem. Phys.* **1957**, *26*, 956. [[CrossRef](#)]
6. Kaner, R.B.; Gilman, J.J.; Tolbert, S.H. Designing superhard materials. *Science* **2005**, *308*, 1268. [[CrossRef](#)]
7. Tian, Y.; Xu, B.; Yu, D.; Ma, Y.; Wang, Y.; Jiang, Y.; Hu, W.; Tang, C.; Gao, Y.; Luo, K.; et al. Ultrahard nanotwinned cubic boron nitride. *Nat. Cell Biol.* **2013**, *493*, 385–388. [[CrossRef](#)]
8. Dubrovinskaia, N.; Solozhenko, V.L.; Miyajima, N.; Dmitriev, V.; Kurakevych, O.O.; Dubrovinsky, L. Superhard nanocomposite of dense polymorphs of boron nitride: Noncarbon material has reached diamond hardness. *Appl. Phys. Lett.* **2007**, *90*, 101912. [[CrossRef](#)]
9. Vepřek, S. The search for novel, superhard materials. *J. Vac. Sci. Technol. A* **1999**, *17*, 2401–2420. [[CrossRef](#)]
10. Wentorf, R.H.; Devries, R.C.; Bundy, F.P. Sintered superhard materials. *Science* **1980**, *208*, 873–880. [[CrossRef](#)] [[PubMed](#)]

11. Vepřek, S. Nanostructured Superhard Materials. In *Handbook of Ceramic Hard Materials*; Riedel, R., Ed.; Wiley-VCH Verlag GmbH: Weinheim, Germany, 2000; pp. 104–139.
12. Wang, P.; He, D.; Wang, L.; Kou, Z.; Li, Y.; Xiong, L.; Hu, Q.; Xu, C.; Lei, L.; Wang, Q.; et al. Diamond-cBN alloy: A universal cutting material. *Appl. Phys. Lett.* **2015**, *107*, 101901. [[CrossRef](#)]
13. Solozhenko, V.L.; Dub, S.N.; Novikov, N.V. Mechanical properties of cubic BC<sub>2</sub>N, a new superhard phase. *Diam. Relat. Mater.* **2001**, *10*, 2228–2231. [[CrossRef](#)]
14. Zhao, Y.; He, D.W.; Daemen, L.L.; Shen, T.D.; Schwarz, R.B.; Zhu, Y.; Bish, D.L.; Huang, J.; Zhang, J.; Shen, G.; et al. Superhard B–C–N materials synthesized in nanostructured bulks. *J. Mater. Res.* **2002**, *17*, 3139. [[CrossRef](#)]
15. Liu, X.; Jia, X.; Zhang, Z.; Zhao, M.; Guo, W.; Huang, G.; Ma, H.-A. Synthesis and characterization of new “BCN” Diamond under high pressure and high temperature conditions. *Cryst. Growth Des.* **2011**, *11*, 1006–1014. [[CrossRef](#)]
16. Liu, A.Y.; Cohen, M.L. Prediction of new low compressibility solids. *Science* **1989**, *245*, 841–842. [[CrossRef](#)]
17. Teter, D.M.; Hemley, R.J. Low-compressibility carbon nitrides. *Science* **1996**, *271*, 53–55. [[CrossRef](#)]
18. Liu, A.; Wentzcovitch, R.M. Stability of carbon nitride solids. *Phys. Rev. B* **1994**, *50*, 10362. [[CrossRef](#)]
19. Wang, H.; He, D.; Tan, N.; Wang, W.; Wang, J.; Dong, H.; Ma, H.; Kou, Z.; Peng, F.; Liu, X.; et al. Note: An anvil-preformed gasket system to extend the pressure range for large volume cubic presses. *Rev. Sci. Instrum.* **2010**, *81*, 116102. [[CrossRef](#)]
20. Walker, D. Lubrication, gasketing, and precision in multianvil experiments. *Am. Mineral.* **1991**, *76*, 1092.
21. Wang, P.; Kumar, R.; Sankaran, E.M.; Qi, X.; Zhang, X.; Popov, D.; Cornelius, A.L.; Li, B.; Zhao, Y.; Wang, L. Vanadium diboride (VB<sub>2</sub>) synthesized at high pressure: Elastic, mechanical, electronic, and magnetic properties and thermal stability. *Inorg. Chem.* **2018**, *57*, 1096–1105. [[CrossRef](#)] [[PubMed](#)]
22. Wang, Y.; Durham, W.B.; Getting, I.C.; Weidner, D.J. The deformation-DIA: A new apparatus for high temperature triaxial deformation to pressures up to 15 GPa. *Rev. Sci. Instrum.* **2003**, *74*, 3002. [[CrossRef](#)]
23. Shatskiy, A.; Katsura, T.; Litasov, K.; Shcherbakova, A.; Borzdov, Y.; Yamazaki, D.; Yoneda, A.; Ohtani, E.; Ito, E. High pressure generation using scaled-up Kawai-cell. *Phys. Earth Planet. Inter.* **2011**, *189*, 92–108. [[CrossRef](#)]
24. Kawai, N.; Endo, S. The generation of ultrahigh hydrostatic pressures by a split sphere apparatus. *Rev. Sci. Instrum.* **1970**, *41*, 1178–1181. [[CrossRef](#)]
25. Andrault, D.; Fiquet, G. Synchrotron radiation and laser heating in a diamond anvil cell. *Rev. Sci. Instrum.* **2001**, *72*, 1283. [[CrossRef](#)]
26. Solozhenko, V.L.; Kurakevych, O.O. New boron subnitride B<sub>13</sub>N<sub>2</sub>: HP-HT synthesis, structure and equation of state. *J. Phys. Conf. Ser.* **2008**, *121*, 062001. [[CrossRef](#)]
27. Sjöström, H.; Stafström, S.; Boman, M.; Sundgren, J.-E. Superhard and elastic carbon nitride thin films having fullerene-like microstructure. *Phys. Rev. Lett.* **1995**, *75*, 1336–1339. [[CrossRef](#)]
28. Zerr, A.; Miehe, G.; Serghiou, G.; Schwarz, M.; Kroke, E.; Riedel, R.; Fieß, H.; Kroll, P.; Boehler, R. Synthesis of cubic silicon nitride. *Nat. Cell Biol.* **1999**, *400*, 340–342. [[CrossRef](#)]
29. Zerr, A.; Kempf, M.; Schwarz, M.; Kroke, E.; Göken, M.; Riedel, R. Elastic moduli and hardness of cubic silicon nitride. *J. Am. Ceram. Soc.* **2004**, *85*, 86–90. [[CrossRef](#)]
30. Hall, O.E. The deformation and ageing of mild steel: III discussion of results. *Proc. Phys. Soc. Sect. B* **1951**, *64*, 747–753. [[CrossRef](#)]
31. Petch, N.J. The orientation relationships between cementite and  $\alpha$ -iron. *Acta Crystallogr.* **1953**, *6*, 96. [[CrossRef](#)]
32. Liu, G.; Kou, Z.; Yan, X.; Lei, L.; Peng, F.; Wang, Q.; Wang, K.; Wang, P.; Li, L.; Li, Y.; et al. Submicron cubic boron nitride as hard as diamond. *Appl. Phys. Lett.* **2015**, *106*, 121901. [[CrossRef](#)]
33. Wang, S.; Antonio, D.; Yu, X.; Zhang, J.; Cornelius, A.L.; He, D.; Zhao, Y. The hardest superconducting metal nitride. *Sci. Rep.* **2015**, *5*, srep13733. [[CrossRef](#)]
34. Dewaele, A.; Loubeyre, P.; Mezouar, M. Equations of state of six metals above 94GPa. *Phys. Rev. B* **2004**, *70*, 094112. [[CrossRef](#)]
35. Srivatsan, T.S.; Ravi, B.G.; Naruka, A.S.; Riester, L.; Petrarolic, M.; Sudarshan, T.S. The microstructure and hardness of molybdenum powders consolidated by plasma pressure compaction. *Powder Technol.* **2001**, *114*, 136–144. [[CrossRef](#)]
36. Oyama, S.T. Introduction to the Chemistry of Transition Metal Carbides and Nitrides. In *The Chemistry of Transition Metal Carbides and Nitrides*; Springer Science and Business Media LLC: London, UK, 1996; pp. 1–27.
37. Schönberg, N.; Overend, W.G.; Munthe-Kaas, A.; Sörensen, N.A. Contributions to the knowledge of the molybdenum-nitrogen and the tungsten-nitrogen systems. *Acta Chem. Scand.* **1954**, *8*, 204–207. [[CrossRef](#)]
38. Choi, D.; Kumta, P.N. Synthesis, structure, and electrochemical characterization of nanocrystalline tantalum and tungsten nitrides. *J. Am. Ceram. Soc.* **2007**, *90*, 3113–3120. [[CrossRef](#)]
39. Wriedt, H.A. The N-W (nitrogen-tungsten) system. *Bull. Alloy. Phase Diagr.* **1989**, *10*, 358–367. [[CrossRef](#)]
40. Lei, L.; He, D. Synthesis of GaN Crystals through solid-state metathesis reaction under high pressure. *Cryst. Growth Des.* **2009**, *9*, 1264–1266. [[CrossRef](#)]
41. Wang, S.; Yu, X.; Lin, Z.; Zhang, R.; He, D.; Qin, J.; Zhu, J.; Han, J.; Wang, L.; Mao, H.-K.; et al. Synthesis, crystal structure, and elastic properties of novel tungsten nitrides. *Chem. Mater.* **2012**, *24*, 3023–3028. [[CrossRef](#)]
42. Chen, M.; Wang, S.; Zhang, J.; He, D.; Zhao, Y. Synthesis of stoichiometric and bulk CrN through a solid-state ion-exchange reaction. *Chem. A Eur. J.* **2012**, *18*, 15459–15463. [[CrossRef](#)] [[PubMed](#)]
43. Wang, S.; Ge, H.; Sun, S.; Zhang, J.; Liu, F.; Wen, X.; Yu, X.; Wang, L.; Zhang, Y.; Xu, H.; et al. A new molybdenum nitride catalyst with rhombohedral MoS<sub>2</sub> structure for hydrogenation applications. *J. Am. Chem. Soc.* **2015**, *137*, 4815–4822. [[CrossRef](#)] [[PubMed](#)]

44. Wang, S.; Yu, X.; Zhang, J.; Wang, L.; Leinenweber, K.; He, D.; Zhao, Y. Synthesis, hardness, and electronic properties of stoichiometric VN and CrN. *Cryst. Growth Des.* **2015**, *16*, 351–358. [[CrossRef](#)]
45. Solozhenko, V.L.; Kurakevych, O.O.; Le Godec, Y. Creation of nanostructures by extreme conditions: High-pressure synthesis of ultrahard nanocrystalline cubic boron nitride. *Adv. Mater.* **2012**, *24*, 1540–1544. [[CrossRef](#)]
46. Hall, H.T. Ultra-high-pressure, high-temperature apparatus: The “Belt”. *Rev. Sci. Instrum.* **1960**, *31*, 125–131. [[CrossRef](#)]
47. Hall, H.T. Some high-pressure, high-temperature apparatus design considerations: Equipment for use at 100,000 atmospheres and 3000 °C. *Rev. Sci. Instrum.* **1958**, *29*, 267. [[CrossRef](#)]
48. Osugi, J.; Shimizu, K.; Inoue, K.; Yasunami, K. A compact cubic anvil high pressure apparatus. *Rev. Phys. Chem. Jpn.* **1964**, *34*, 1–6.
49. Wang, F.; He, D.; Fang, L.; Chen, X.; Li, Y.; Zhang, W.; Zhang, J.; Kou, Z.; Peng, F. Design and assembly of split-sphere high pressure apparatus based on the hinge-type cubic-anvil press. *Acta Phys. Sin.* **2008**, *57*, 5429–5434.
50. Wang, W.; He, D.; Wang, H.; Wang, F.; Dong, H.; Chen, H.; Li, Y.; Zhang, J.; Wang, S.; Kou, Z.; et al. Research on pressure generation efficiency of 6–8 type multianvil high pressure apparatus. *Acta Phys. Sin.* **2010**, *59*, 3017–3115.
51. Onodera, A.; Ohtani, A. Fixed points for pressure calibration above 100 kbars related to semiconductor-metal transitions. *J. Appl. Phys.* **1980**, *51*, 2581. [[CrossRef](#)]
52. Wang, P.; Wang, Y.; Wang, L.; Zhang, X.; Yu, X.; Zhu, J.; Wang, S.; Qin, J.; Leinenweber, K.; Chen, H.; et al. Elastic, magnetic and electronic properties of iridium phosphide Ir<sub>2</sub>P. *Sci. Rep.* **2016**, *6*, 21787. [[CrossRef](#)]
53. Xu, C.; He, D.; Wang, H.; Guan, J.; Liu, C.; Peng, F.; Wang, W.; Kou, Z.; He, K.; Yan, X.; et al. Nano-polycrystalline diamond formation under ultra-high pressure. *Int. J. Refract. Met. Hard Mater.* **2013**, *36*, 232–237. [[CrossRef](#)]
54. Liu, J.; Zhan, G.; Wang, Q.; Yan, X.; Liu, F.; Wang, P.; Lei, L.; Peng, F.; Kou, Z.; He, D. Superstrong micro-grained polycrystalline diamond compact through work hardening under high pressure. *Appl. Phys. Lett.* **2018**, *112*, 061901. [[CrossRef](#)]
55. Wang, W.; He, D.; Tang, M.; Li, F.; Liu, L.; Bi, Y. Superhard composites of cubic silicon nitride and diamond. *Diam. Relat. Mater.* **2012**, *27–28*, 49–53. [[CrossRef](#)]
56. Tang, M.; He, D.; Wang, W.; Wang, H.; Xu, C.; Li, F.; Guan, J. Superhard solid solutions of diamond and cubic boron nitride. *Scr. Mater.* **2012**, *66*, 781–784. [[CrossRef](#)]
57. Solozhenko, V.L.; Andrault, D.; Fiquet, G.; Mezouar, M.; Rubie, D.C. Synthesis of superhard cubic BC<sub>2</sub>N. *Appl. Phys. Lett.* **2001**, *78*, 1385–1387. [[CrossRef](#)]
58. Badzian, A.R. Cubic boron nitride—Diamond mixed crystals. *Mater. Res. Bull.* **1981**, *16*, 1385–1393. [[CrossRef](#)]
59. Sasaki, T.; Akaishi, M.; Yamaoka, S.; Fujiki, Y.; Oikawa, T. Simultaneous crystallization of diamond and cubic boron nitride from the graphite relative boron carbide nitride (BC<sub>2</sub>N) under high pressure/high temperature conditions. *Chem. Mater.* **1993**, *5*, 695–699. [[CrossRef](#)]
60. Nakano, S.; Akaishi, M.; Sasaki, T.; Yamaoka, S. Segregative crystallization of several diamond-like phases from the graphitic BC<sub>2</sub>N without an Additive at 7.7 GPa. *Chem. Mater.* **1994**, *6*, 2246–2251. [[CrossRef](#)]
61. Knittle, E.; Kaner, R.B.; Jeanloz, R.; Cohen, M.L. High-pressure synthesis, characterization, and equation of state of cubic C-BN solid solutions. *Phys. Rev. B* **1995**, *51*, 12149–12156. [[CrossRef](#)]
62. Solozhenko, V.L.; Le Godec, Y.; Kurakevych, O.O. Solid-state synthesis of boron subnitride, B<sub>6</sub>N: Myth or reality? *Comptes Rendus Chimie* **2006**, *9*, 1472–1475. [[CrossRef](#)]
63. Vogel, S.; Bykov, M.; Bykova, E.; Wendl, S.; Kloß, S.D.; Pakhomova, A.; Dubrovinskaia, N.; Dubrovinsky, L.; Schnick, W. Boron phosphorus nitride at extremes: PN<sub>6</sub> octahedra in the high-pressure polymorph β-BP<sub>3</sub>N<sub>6</sub>. *Angew. Chem. Int. Ed.* **2019**, *58*, 9060–9063. [[CrossRef](#)]
64. Jansen, M.; Schön, J.C.; Van Wüllen, L. The route to the structure determination of amorphous solids: A case study of the ceramic Si<sub>3</sub>B<sub>3</sub>N<sub>6</sub>. *Chem. Int. Ed.* **2006**, *45*, 4244–4263. [[CrossRef](#)]
65. Vogel, S.; Buda, A.T.; Schnick, W. United in nitride: The highly condensed boron phosphorus nitride BP<sub>3</sub>N. *Angew. Chem. Int. Ed.* **2018**, *57*, 13202–13205. [[CrossRef](#)]
66. Landskron, K.; Huppertz, H.; Senker, J.; Schnick, W. High-pressure synthesis of γ-P<sub>3</sub>N<sub>5</sub> at 11 GPa and 1500 °C in a multianvil assembly: A binary phosphorus(V) nitride with a three-dimensional network structure from PN<sub>4</sub> tetrahedra and tetragonal PN<sub>5</sub> pyramids. *Angew. Chem. Int. Ed.* **2001**, *40*, 2643. [[CrossRef](#)]
67. Landskron, K.; Huppertz, H.; Senker, J.; Schnick, W.Z. Multianvil synthesis, X-ray powder diffraction analysis, <sup>31</sup>P-MAS-NMR, and FTIR spectroscopy as well as material properties of γ-P<sub>3</sub>N<sub>5</sub>, a high-pressure polymorph of binary phosphorus(V) nitride, built up from distorted PN<sub>5</sub> square pyramids and PN<sub>4</sub> tetrahedra. *Anorg. Allg. Chem.* **2002**, *628*, 1465–1471. [[CrossRef](#)]
68. Andrievski, R.A. Superhard materials based on nanostructured high-melting point compounds: Achievements and perspectives. *Int. J. Refract. Met. H.* **2001**, *19*, 447–452. [[CrossRef](#)]
69. Chen, M.; Ma, E.; Hemker, K.J.; Sheng, H.; Wang, Y.; Cheng, X. Deformation Twinning in nanocrystalline aluminum. *Science* **2003**, *300*, 1275–1277. [[CrossRef](#)]
70. Lu, L.; Shen, Y.; Chen, X.; Qian, L.; Lu, K. ultrahigh strength and high electrical conductivity in copper. *Science* **2004**, *304*, 422–426. [[CrossRef](#)] [[PubMed](#)]
71. Young, A.F.; Sanloup, C.; Gregoryanz, E.; Scandolo, S.; Hemley, R.J.; Mao, H. Synthesis of novel transition metal nitrides IrN<sub>2</sub> and OsN<sub>2</sub>. *Phys. Rev. Lett.* **2006**, *96*, 155501. [[CrossRef](#)] [[PubMed](#)]
72. Zerr, A.; Riedel, R.; Sekine, T.; Lowther, J.E.; Ching, W.Y.; Tanaka, I. Recent advances in new hard high-pressure nitrides. *Adv. Mater.* **2006**, *18*, 2933–2948. [[CrossRef](#)]

73. Gregoryanz, E.; Sanloup, C.; Somayazulu, M.S.; Badro, J.; Fiquet, G.; Mao, H.-K.; Hemley, R.J. Synthesis and characterization of a binary noble metal nitride. *Nat. Mater.* **2004**, *3*, 294–297. [[CrossRef](#)] [[PubMed](#)]
74. Kroll, P. Hafnium nitride with thorium phosphide structure: Physical properties and an assessment of the Hf-N, Zr-N, and Ti-N phase diagrams at high pressures and temperatures. *Phys. Rev. Lett.* **2003**, *90*, 125501. [[CrossRef](#)] [[PubMed](#)]
75. Jhi, S.-H.; Ihm, J.; Louie, S.G.; Cohen, M.L. Electronic mechanism of hardness enhancement in transition-metal carbonitrides. *Nat. Cell Biol.* **1999**, *399*, 132–134. [[CrossRef](#)]
76. Crowhurst, J.C.; Goncharov, A.F.; Sadigh, B.; Evans, C.L.; Morrall, P.G.; Ferreira, J.L.; Nelson, A. Synthesis and characterization of the nitrides of platinum and iridium. *Science* **2006**, *311*, 1275–1278. [[CrossRef](#)] [[PubMed](#)]
77. Khazaei, M.; Arai, M.; Sasaki, T.; Chung, C.-Y.; Venkataramanan, N.S.; Estili, M.; Sakka, Y.; Kawazoe, Y. Novel electronic and magnetic properties of two-dimensional transition metal carbides and nitrides. *Adv. Funct. Mater.* **2013**, *23*, 2185–2192. [[CrossRef](#)]
78. Lei, L.; Yin, W.; Jiang, X.; Lin, S.; He, D. Synthetic route to metal nitrides: High-pressure solid-state metathesis reaction. *Inorg. Chem.* **2013**, *52*, 13356–13362. [[CrossRef](#)]
79. Herle, P.S.; Hegde, M.; Vasathacharya, N.; Philip, S.; Rao, M.R.; Sripathi, T. Synthesis of TiN, VN, and CrN from ammonolysis of TiS<sub>2</sub>, VS<sub>2</sub>, and Cr<sub>2</sub>S<sub>3</sub>. *Solid State Chem.* **1997**, *134*, 120–127. [[CrossRef](#)]
80. Yin, W.; Lei, L.; Jiang, X.; Liu, P.; Liu, F.; Li, Y.; Peng, F.; He, D. High pressure synthesis and properties studies on spherical bulk e-Fe<sub>3</sub>N. *High. Press. Res.* **2014**, *34*, 317–326. [[CrossRef](#)]
81. Jiang, X.; Lei, L.; Hu, Q.; Feng, Z.C.; He, D. High-pressure Raman spectroscopy of Re<sub>3</sub>N crystals. *Solid State Commun.* **2015**, *201*, 107–110. [[CrossRef](#)]
82. Qian, J.; Daemen, L.; Zhao, Y. Hardness and fracture toughness of moissanite. *Diam. Relat. Mater.* **2005**, *14*, 1669–1672. [[CrossRef](#)]
83. Gao, F.; He, J.; Wu, E.; Liu, S.; Yu, D.; Li, D.; Zhang, S.; Tian, Y. Hardness of covalent crystals. *Phys. Rev. Lett.* **2003**, *91*, 015502. [[CrossRef](#)]
84. Vepřek, S.; Reiprich, S.; Shizhi, L. Superhard nanocrystalline composite materials: The TiN/Si<sub>3</sub>N<sub>4</sub> system. *Appl. Phys. Lett.* **1995**, *66*, 2640–2642. [[CrossRef](#)]
85. Zhang, S.; Sun, D.; Fu, Y.; Du, H. Recent advances of superhard nanocomposite coatings: A review. *Surf. Coat. Technol.* **2003**, *167*, 113–119. [[CrossRef](#)]
86. Zhu, Y.; Liao, X.; Wu, X. Deformation twinning in nanocrystalline materials. *Prog. Mater. Sci.* **2012**, *57*, 1–62. [[CrossRef](#)]
87. Kunimoto, T.; Irifune, T. Pressure generation to 125 GPa using a 6-8-2 type multianvil apparatus with nano-polycrystalline diamond anvils. *J. Phys. Conf. Ser.* **2010**, *215*, 012190. [[CrossRef](#)]
88. Sun, W.; Bartel, C.J.; Arca, E.; Bauers, S.R.; Matthews, B.; Orvañanos, B.; Chen, B.; Toney, M.F.; Schelhas, L.T.; Tumas, W.; et al. A map of the inorganic ternary metal nitrides. *Nat. Mater.* **2019**, *18*, 732–739. [[CrossRef](#)] [[PubMed](#)]
89. McSkimin, H.J.; Andreatch, P. Elastic moduli of diamond as a function of pressure and temperature. *J. Appl. Phys.* **1972**, *43*, 2944–2948. [[CrossRef](#)]
90. Grimsditch, M.; Zouboulis, E.S.; Polian, A. Elastic constants of boron nitride. *J. Appl. Phys.* **1994**, *76*, 832–834. [[CrossRef](#)]
91. Liu, Y.; Zhan, G.; Wang, Q.; He, D.; Zhang, J.; Liang, A.; Moellendick, T.E.; Zhao, L.; Li, X. Hardness of polycrystalline wurtzite boron nitride (wBN) compacts. *Sci. Rep.* **2019**, *9*, 1–6. [[CrossRef](#)]
92. Gao, F. Theoretical model of intrinsic hardness. *Phys. Rev. B* **2006**, *73*, 132104. [[CrossRef](#)]
93. Becher, P.F.; Sun, E.Y.; Plucknett, K.; Alexander, K.B.; Hsueh, C.-H.; Lin, H.-T.; Waters, S.B.; Westmoreland, C.G.; Kang, E.-S.; Hirao, K.; et al. Microstructural design of silicon nitride with improved fracture toughness: I, effects of grain shape and size. *J. Am. Ceram. Soc.* **2005**, *81*, 2821–2830. [[CrossRef](#)]
94. Soignard, E.; Somayazulu, M.; Dong, J.; Sankey, O.F.; McMillan, P.F. High pressure-high temperature synthesis and elasticity of the cubic nitride spinel  $\gamma$ -Si<sub>3</sub>N<sub>4</sub>. *Phys. Condens. Matter.* **2001**, *13*, 557–563. [[CrossRef](#)]
95. Dong, H.; He, D.; Duffy, T.S.; Zhao, Y. Elastic moduli and strength of nanocrystalline cubic BC<sub>2</sub>N from X-ray diffraction under nonhydrostatic compression. *Phys. Rev. B* **2009**, *79*, 014105. [[CrossRef](#)]
96. Jauberteau, I.; Bessaudou, A.; Mayet, R.; Cornette, J.; Jauberteau, J.L.; Carles, P.; Merle-Mejean, T. Molybdenum nitride films: Crystal Structures, synthesis, mechanical, electrical and some other properties. *Coatings* **2015**, *5*, 656–687. [[CrossRef](#)]
97. Bykov, M.; Chariton, S.; Fei, H.; Fedotenko, T.; Aprilis, G.; Ponomareva, A.V.; Tasnádi, F.; Abrikosov, I.A.; Merle, B.; Feldner, P.; et al. High-pressure synthesis of ultraincompressible hard rhenium nitride pernitride Re<sub>2</sub>(N<sub>2</sub>)(N)<sub>2</sub> stable at ambient conditions. *Nat. Commun.* **2019**, *10*, 2994. [[CrossRef](#)] [[PubMed](#)]
98. Friedrich, A.; Winkler, B.; Bayarjargal, L.; Morgenroth, W.; Juarez-Arellano, E.A.; Milman, V.; Refson, K.; Kunz, M.; Chen, K. Novel Rhenium Nitrides. *Phys. Rev. Lett.* **2010**, *105*, 085504. [[CrossRef](#)] [[PubMed](#)]
99. Chen, X.-Q.; Niu, H.; Li, D.; Li, Y. Modeling hardness of polycrystalline materials and bulk metallic glasses. *Intermetallics* **2011**, *19*, 1275–1281. [[CrossRef](#)]
100. Tian, Y.; Xu, B.; Zhao, Z. Microscopic theory of hardness and design of novel superhard crystals. *Int. J. Refract. Met. Hard Mater.* **2012**, *33*, 93–106. [[CrossRef](#)]
101. Chen, X.-J.; Struzhkin, V.V.; Wu, Z.; Somayazulu, M.; Qian, J.; Kung, S.; Christensen, A.N.; Zhao, Y.; Cohen, R.E.; Mao, H.-K.; et al. Hard superconducting nitrides. *Proc. Natl. Acad. Sci. USA* **2005**, *102*, 3198–3201. [[CrossRef](#)]
102. Guo, X.; Li, L.; Liu, Z.; Yu, D.; He, J.; Liu, R.; Xu, B.; Tian, Y.; Wang, H.-T. Hardness of covalent compounds: Roles of metallic component and d valence electrons. *J. Appl. Phys.* **2008**, *104*, 023503. [[CrossRef](#)]

103. Soignard, E.; Shebanova, O.; McMillan, P.F. Compressibility measurements and phonon spectra of hexagonal transition-metal nitrides at high pressure:  $\epsilon$ -TaN,  $\delta$ -MoN, and Cr<sub>2</sub>N. *Phys. Rev. B* **2007**, *75*, 014104. [[CrossRef](#)]
104. Zou, Y.; Wang, X.; Chen, T.; Li, X.; Qi, X.; Welch, D.; Zhu, P.; Liu, B.; Cui, T.; Li, B. Hexagonal-structured  $\epsilon$ -NbN: Ultra-incompressibility, high shear rigidity, and a possible hard superconducting material. *Sci. Rep.* **2015**, *5*, 10811. [[CrossRef](#)]
105. Wang, S.; Yu, X.; Zhang, J.; Chen, M.; Zhu, J.; Wang, L.; He, D.; Lin, Z.; Zhang, R.; Leinenweber, K.; et al. Experimental invalidation of phase-transition-induced elastic softening in CrN. *Phys. Rev. B* **2012**, *86*, 064111. [[CrossRef](#)]
106. Kim, J.O.; Achenbach, J.D.; Mirkarimi, P.B.; Shinn, M.; Barnett, S.A. Elastic constants of single-crystal transition-metal nitride films measured by line-focus acoustic microscopy. *J. Appl. Phys.* **1992**, *72*, 1805. [[CrossRef](#)]
107. Drory, M.D.; Ager, J.W.; Suski, T.; Grzegory, I.; Porowski, S. Hardness and fracture toughness of bulk single crystal gallium nitride. *Appl. Phys. Lett.* **1996**, *69*, 4044–4046. [[CrossRef](#)]
108. Ma, D.; Kou, Z.; Liu, Y.; Wang, Y.; Gao, S.; Luo, X.; Li, W.; Wang, Y.; Du, Y.; Lei, L. Sub-micron binderless tungsten carbide sintering behavior under high pressure and high temperature. *Int. J. Refract. Met. Hard Mater.* **2016**, *54*, 427–432. [[CrossRef](#)]